THESIS

QUANTIFYING THE IMPACT OF CLIMATE CHANGE AND LAND USE CHANGE ON SURFACE-SUBSURFACE NUTRIENT DYNAMICS IN A CHESAPEAKE BAY WATERSHED

Submitted by

Avalokita Tuladhar

Department of Civil and Environmental Engineering

In partial fulfillment of the requirements

For the Degree of Master of Science

Colorado State University

Fort Collins, Colorado

Fall 2023

Master's Committee:

Advisor: Ryan T. Bailey
Co-Advisor: Mohana Sundaram Shanmugam

Ryan Smith
Matthew Ross

ABSTRACT

QUANTIFYING THE IMPACT OF CLIMATE CHANGE AND LAND USE CHANGE ON SURFACE-SUBSURFACE NUTRIENT DYNAMICS IN A CHESAPEAKE BAY WATERSHED

Nutrients such as nitrogen can be harmful to aquatic organisms when loaded to receive water in excessive amounts. Climate change, through possible increases in temperature and variable rainfall, may cause changes in nutrient loading patterns from watersheds. This study assesses the potential impact of climate and land use change on nitrate (NO_3) loading in the Nanticoke River Watershed (NRW), Chesapeake Bay region, USA, using an updated version of SWAT+ watershed model that simulates groundwater nitrate fate and transport in a physically based spatially distributed manner. The nutrient loadings from the NRW eventually drain into the Chesapeake Bay, exacerbating eutrophication. The model was simulated for the 2000-2015 time, and tested against measured streamflow, in-stream nitrate loadings, and groundwater head at various stream gages and monitoring wells. Once tested, the model was used to simulate changes in hydrological and nitrate fluxes under two future climates, according to Representative Concentration Pathways (RCP) 4.5 and 8.5, and land use changes as projected by USGS's FORE-SCE model. The projected results show that in the future climate change is to be responsible for an 18-34% and 22-33% decrease in annual average streamflow and a 4-22% and 4-11% decrease in annual average nitrate loading as projected under RCP 4.5 and RCP 8.5 scenarios for future timelines (near 2024-2048, mid 2049-2073 and far future 2074-2099), respectively. The overall decrease in future streamflow is due to higher temperatures resulting in higher evapotranspiration during summer months, offsetting the additional precipitation. The decrease in nitrate loading in the channel is influenced by lower runoff, and elevated nitrate concentration in the soil, leading to increased leaching into groundwater. This surge in soil nitrate concentration results from reduced plant uptake of nitrate due to decreased plant growth/lower crop yields. The stunted plant growth is due to reduced mineralization of nitrogen in the soil which, in turn, is linked to decreasing soil water content and water stress from higher surface temperatures. As compared to the influence of climate, land use change resulted in a minor decrease in future nitrate loading. These results and insights can be used in future nutrient management for similar landscapes. In addition, we show that the updated SWAT+ model can be a useful tool in

quantifying and investigating nitrate fate and transport dynamics in coupled surface-soil-aquifer-channel systems, particularly for systems with a strong hydraulic connection between the unconfined aquifer and channel network.

TABLE OF CONTENTS

LIST OF TABLES

LIST OF FIGURES

CHAPTER 1- INTRODUCTION

Excessive loads of nutrients such as nitrogen (N) and phosphorus (P) from watersheds drive eutrophication in estuaries worldwide (Adams et al., 2020; Oelsner & Stets, 2019; Rabalais et al., 2009; Sinha et al., 2017; Wurtsbaugh et al., 2019). These loads originate from anthropogenic sources such as fertilizer from cultivated areas and wastewater treatment plant (WWTP) effluent from urban areas. Whereas WWTP effluent loads are point sources to streams, rivers, and lakes, loads from cultivated areas often enter receiving waters as non-point diffusive mass, via surface runoff, soil lateral flow, tile drainage outflow, and groundwater discharge. To estimate the magnitude, location, and timing of both point source and non-point source nutrient loads into river systems, watershed water quality models are often used, such as the Soil & Water Assessment Tool (SWAT) (Arnold et al., 1998); SWAT+ (Bieger et al., 2017), the restructured version of SWAT, which provides a more detailed connection between hydrologic objects in a watershed system; the Hydrological Simulation Program – Fortran (HSPF) (Duda et al., 2012); and SWAT-MODFLOW-RT3D (Wei et al., 2019; Wei & Bailey, 2021), a linkage between SWAT and the USGS groundwater flow model MODFLOW that simulates N and P transport in the coupled surface-subsurface system.

Future management of nutrient loads must account for possible changes in climate patterns and land use, which may have a significant impact on water quality in watershed systems (Buonocore et al., 2021; S. Shrestha et al., 2018; El-Khoury et al., 2015; M. K. Shrestha et al., 2017; Mehdi et al., 2015; Tu, 2009; Khoi et al., 2019). Climate change might lead to an increase in nutrient loadings (Meier et al., 2019; Mukundan et al., 2020; Pihlainen et al., 2020; Yasarer et al., 2017) or decrease in nutrient loadings (M. K. Shrestha et al., 2017b; S. Shrestha et al., 2018). For example, changing precipitation rates and patterns can influence in-river nutrient loading, as either increased streamflow or decrease streamflow changes the load of nitrogen in a watershed system along with changes in the seasonality of loading (Sperotto et al., 2019) . S. Shrestha et al., 2018 and Kalcic et al., 2019 noted a decrease in future nitrate loading due to projected declines in precipitation and associated streamflow generation, whereas R. R. Shrestha et al., 2012 found a projected increase in runoff and nutrient loads to river due to increases in precipitation. Changes in temperature can also influence nitrogen dynamics in a soil-aquifer-channel system, as rising temperatures may result in earlier snowmelt peaks that affect the timing of nutrient release from snow-covered areas, potentially influencing nutrient loading patterns. Changing temperatures can also affect crop growth and microbial behavior, modifying nitrogen cycling in the root zone of soil profile. The rapid maturation of the plants, in comparison to the

baseline, can be attributed to the significant impact of temperature and carbon dioxide levels on their growth. However, there are also cases when, although the carbon dioxide concentrations are elevated, significant temperature led to increase in temperature-related stress, resulting in a reduction in plant size and the uptake of phosphorus (Culbertson et al., 2016). In contrast, a decrease in sediment and nutrient loads might occur due to residue or increase in plant cover (Xie & Ringler, 2017).

Land use changes can also have major impacts on nitrogen movement and loading within watersheds. Jordan et al. (2018) studied the effect of land use on estuarine water quality via field sampling and revealed a significant correlation between croplands, developed lands, and critical water quality parameters like Total Nitrogen, Ammonia, and dissolved inorganic nitrogen. An extensive review was done by Camara et al., (2019) to study the relationship between land use and water quality in Malaysia, indicating that agricultural and forest-related activities mainly influence water quality by positively correlating with physical and chemical indicators. Conversely, urban development primarily impacts water quality by altering hydrological processes like runoff and erosion. A study done by Baker & Miller (2013) discuss how the reduction in forested areas in the uplands resulted in decreased infiltration due to factors such as reduced surface roughness and litter. This results in a larger portion of rainfall being transformed into surface runoff instead of permeating the soil and replenishing the regional aquifer, therefore influencing the water quality. To assist with nutrient management, the combined effect of climate and land use changes on nutrient loading and nutrient dynamics in a watershed system should be assessed. Watershed water quality models can be valuable tools in this endeavor.

In this study, we quantify the impact of future climate and land use on nitrate (NO_3) fate and transport dynamics in the coupled surface-subsurface system of a managed watershed. Specifically, we seek to quantify the changes in nitrate loadings in a watershed channel network as compared to historical conditions, and determine the internal causes for these changes, such as crop, soil, and aquifer hydro-chemical processes. To accomplish this objective, we use the SWAT+ model with the newly developed *gwflow* module option, which simulates groundwater storage, flow, and interaction with surface water features in a physically based spatially distributed manner. Furthermore, we amend the *gwflow* module code to simulate the fate and transport of nitrate in the aquifer system, subject to advection, dispersion, denitrification, and mass input/output from/to other SWAT+ features such as soils, channels, and reservoirs. The resulting updated SWAT+ model provides a holistic approach to simulating nitrate fate and transport in a coupled surface-subsurface watershed system. We use the Nanticoke River Watershed (2,173 km^2),

a tributary watershed to the Chesapeake Bay, as a demonstration case, due to the regional problem of high nutrient loading (Ator et al., 2011; Beegle, 2013; Clune et al., 2021) and the close proximity of groundwater to land surface and the channel network, leading to strong channel-aquifer connections (Sanford et al., 2012). Nutrient loading within watersheds of the Chesapeake Bay region has been investigated and quantified using several other process-based (HSPF- Sarkar et al., 2019; Shenk & Linker, 2013) and statistical modeling tools (GAMs - Beck & Murphy, 2017; Murphy et al., 2019; SPARROW - Ator et al., 2019; Brakebill et al., 2010; Miller et al., 2020; Preston et al., 2009). However, HSPF does not simulate groundwater flow and transport in a physically based manner, and the statistical models do not incorporate detailed surface-subsurface, time-dependent processes that can be investigated in scenarios such as future climate, future land use, and combinations of management practices. Therefore, in addition to providing a new general tool for quantifying impacts on nutrient dynamics in a coupled surface-subsurface system, we also provide a novel tool for use in the Chesapeake Bay watershed system.

The SWAT+ model for this watershed is tested against measured streamflow, in-stream nitrate loadings, and groundwater head at various stream gages and monitoring wells. We then run the model under future climate and land use conditions, to explore the impact on nitrate mass and concentration within each hydrologic feature, and mass fluxes between features. We also explore the causes for these changes. We note that the based SWAT+ model for the Nanticoke River Watershed was developed in R. T. Bailey et al., 2023. However, the presented model was not calibrated, and did not include nitrate transport in the aquifer system.

CHAPTER 2- METHODS

2.1 Study Region

The Nanticoke River Watershed (NRW) (**Figure 1**) is within the Mid-Atlantic region of the United States of America. The Nanticoke watershed encompasses over 2,173 km^2 and stretches across Maryland and Delaware. The watershed is a part of the eastern shore of the Chesapeake Bay watershed. The climate of the region is humid subtropical climate. The average temperature in July (warmest month) is 24 °C and the average temperature in January (coolest month) is 2 °C. The annual precipitation is about 1200 mm. The land use/cover characteristics for the watershed, derived from National Land Cover Database with a resolution of 30 m, are summarized in **Table 1**. As seen in **Table 1**, the NRW is an agriculturally dominated watershed, cultivating mainly corn and soybeans. Forest and wetlands cover the remainder of the watershed. In terms of surface geology, the whole watershed is classified under fine-detrital and the river as alluvial, with a shallow unconfined aquifer in connection with the channel network. The highest elevation in the watershed is 37 m (**Figure 1**). The watershed is drained by the Nanticoke River, with tributaries Cow Creek, Jack Creek Wapremander Creek, Marshyhope Creek, Gravelly Fork, Gum Branch, and Broad Creek. Groundwater in the unconfined aquifer moves horizontally until it reaches a stream or ditch, at which point it can resurface as baseflow into the surface drainage system.

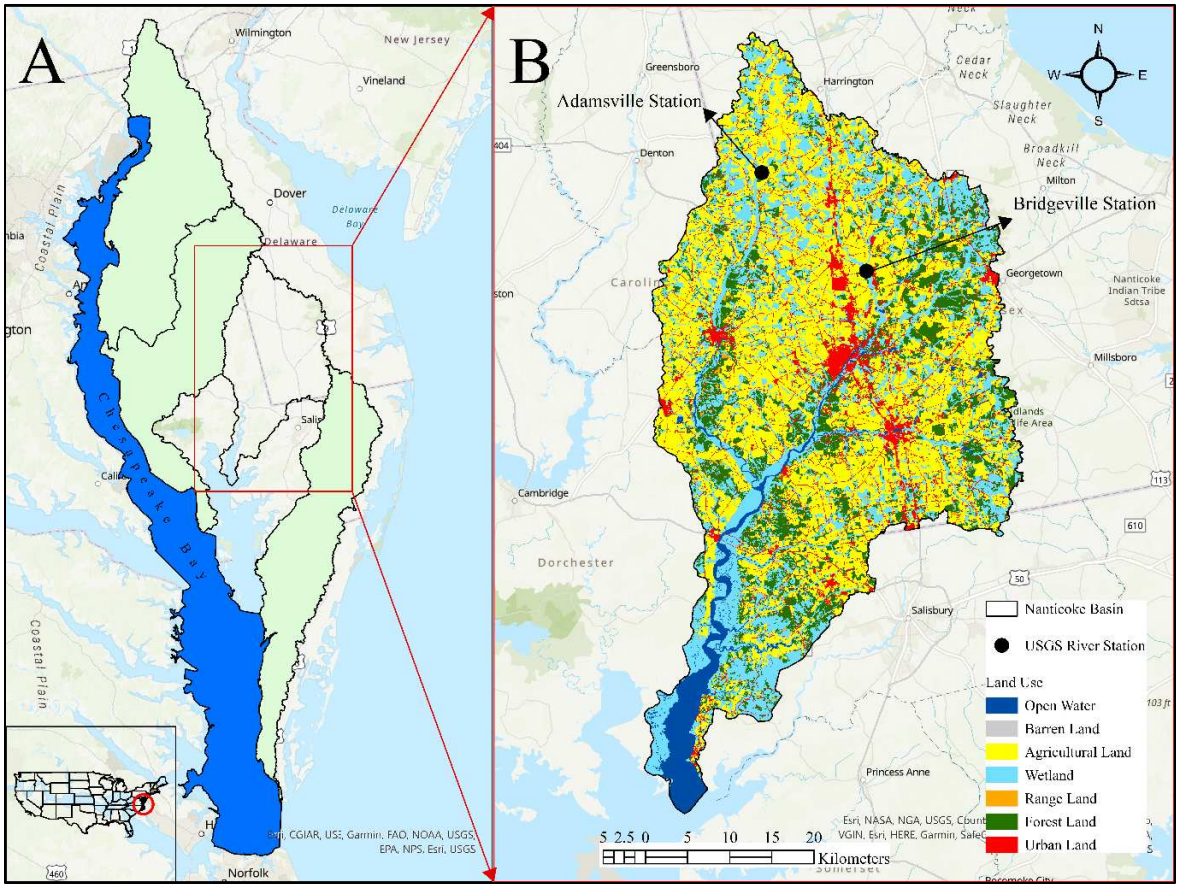

Figure 1: (A) Location of Nanticoke River Watershed within the Chesapeake Bay region; (B) Map of land use in the Nanticoke River Watershed.

Table 1: Land use classification for Nanticoke River Basin.

Land use type	**% Coverage**
Agricultural Land	44.16
Wetlands	26.68
Forest Land	15.11
Developed Land	8.74
Open Water	4.43
Range Land	0.81
Barren Land	0.06

2.2 Modeling Approach: SWAT+ model for the Nanticoke River Watershed

2.2.1 SWAT+ Theory

SWAT+ (Bieger et al., 2017) is a semi-distributed, continuous-in-time hydrologic model that can be applied to watersheds of varying spatial scale. It is a restructured version of the original Soil and Water Assessment Tool (Srinivasan et al., 1998) designed to provide flexible and more accurate hydrologic connectivity between objects such as hydrologic response units (HRUs; unique spatial areas of soil type, topographic slope, and land use), channels,

reservoirs, ponds, wetlands, and aquifers. For each daily time step, water, nutrient, and sediment mass balance is applied to each object in the watershed, with hydrographs and mass fluxes passed between objects in transfer processes such as surface runoff, soil lateral flow, tile drainage outflow, recharge, groundwater discharge, stream and reservoir seepage, and channel routing. Decision tables and water allocation routines are used to trigger management events, such as crop operations, irrigation, and reservoir release. The SWAT+ source code (Fortran) and tools for model calibration, sensitivity analysis, and uncertainty analysis are available at https://swat.tamu.edu/software/plus/. The SWAT+ model also simulates nutrient (N, P) cycling and loading to streams, crop growth, and sediment transport. For nutrient fate and transport, mass balance equations are applied for each daily time step to soil layers, land surface routing, aquifers, and channels. The model has been applied recently for climate and land use impacts (Kiprotich et al., 2021), reservoir operation (Wu et al., 2020), crop management (Nkwasa et al., 2022), groundwater flow and groundwater surface water interaction (R. T. Bailey, Park, et al., 2020), water balance (Pulighe et al., 2021).

2.2.2 gwflow module for SWAT+

The SWAT+ code, like the original SWAT code, uses a simplified representation of aquifer systems to compute groundwater storage and groundwater discharge to channels. Simplifications include homogeneous properties within an aquifer; discharge to channels based on steady flow conditions and user-defined thresholds; and no groundwater flow between adjacent aquifers. Aquifers are treated as isolated objects within a watershed that interact with surface features (soils, reservoirs, channels), but not with each other. While the original groundwater module has been used successfully in many watershed settings to estimate baseflow, sometimes observed baseflow patterns are not replicated due to lack of gradient-based groundwater hydrology. Furthermore, regional groundwater flow patterns and localized effects such as head drawdown due to groundwater pumping, cannot be simulated.

To improve the representation of groundwater hydrology in SWAT+, (R. T. Bailey, Bieger, et al., 2020) created the *gwflow* module for SWAT+. This module, used in placed of the original groundwater module and called as a subroutine within the SWAT+ modeling code, simulates groundwater storage, groundwater head, and interactions with surface water objects in a physically based spatially distributed manner for the unconfined aquifer system of the watershed. **Figure 2** shows the hydrologic processes simulated by SWAT+, when the *gwflow* module is active. Specific processes and interactions simulated by the *gwflow* module include recharge from HRUs, groundwater ET, groundwater discharge to channels and seepage from channels, tile drainage outflow to channels, groundwater flow

within a heterogeneous aquifer, flow across the watershed boundary, groundwater pumping for irrigation and other specified demands, and reservoir exchange.

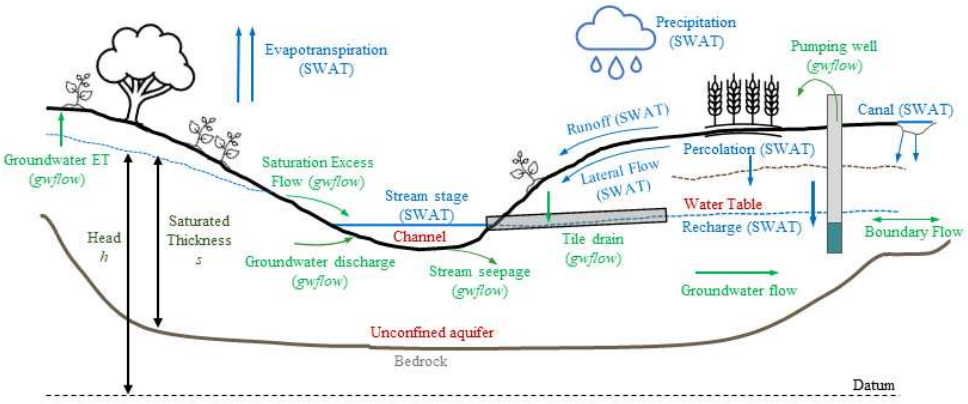

Figure 2: Schematic Representation of hydrologic and nutrient fluxes in the SWAT+ model, using the *gwflow* module.

The *gwflow* module uses a collection of grid cells that span the spatial extent of the watershed, with each cell representing a volume of aquifer. **Figure 3** shows the grid used for the Nanticoke River Watershed, in this study. For each cell, groundwater storage is updated during each daily time step of the model simulation, based on the cell's groundwater inflow (sources) and outflows (sinks) for the day. For a single cell, the equation to update groundwater storage V at time $n+1$ from the previous storage at time n is:

$$V_{(i,j)}^{(n+1)} = V_{(i,j)}^{n} + \left(\sum sources_{(i,j)}^{n} - \sum sinks_{(i,j)}^{n} \pm lateral\ flow_{(i,j)}^{n} \right) \left(t^{(n+1)} - t^{n} \right) \quad (1)$$

where n represents time; i and j represent position (row, column) within the grid; *sources* include recharge from HRUs, seepage from channels, and seepage from reservoirs; *sinks* include groundwater ET if the water table is above a specified extinction depth, discharge to channels and reservoirs, tile drainage outflow to channels, groundwater pumping to HRUs for irrigation, transfer to soil water if the water table is within the soil profile, and saturation excess flow to channels if the water table rises above the ground surface; and *lateral flow* is flow to/from the cell to/from the four neighboring cells (north, south, east, west). After groundwater storage is updated, saturated thickness and groundwater head for the cell are computed using the cells' area and specific yield.

Equations to compute each source/sink are provided in Bailey et al. (2020) and Bailey et al. (2022). Exchange with channels, exchange with reservoirs, tile drainage outflow, and lateral flow are computed using Darcy's Law. Hence, inputs for the *gwflow* module include, for each cell: initial groundwater head (m), aquifer thickness (m) (ground

surface to bedrock), aquifer hydraulic conductivity K (m/day), and aquifer specific yield S_y. If the cell is intersected with channels, reservoirs, or tile drains, then additional parameters are needed: channel bed K and thickness (m); reservoir bed K and thickness (m); and tile drain K and depth below ground surface (m). Spatial connections between cells and HRUs, channels, and reservoirs are performed using a GIS, then stored in a set of *gwflow* input files that are read in at the beginning of the SWAT+ simulation. During the simulation, system-response (groundwater head) and flux variables are written to output files on a daily and annual basis. Total model volumes for each source/sink type are normalized by watershed area and written as depths (mm), along with the water balance error that compares total change in groundwater storage during the day with the summation of all sources and sinks. Cell-by-cell values for the year (m^3/yr) are written for each flux type, to enable the creation of maps that show spatial variability in groundwater sources and sinks. The user can specify output times for cell-by-cell groundwater head (m), to make maps of water table elevation.

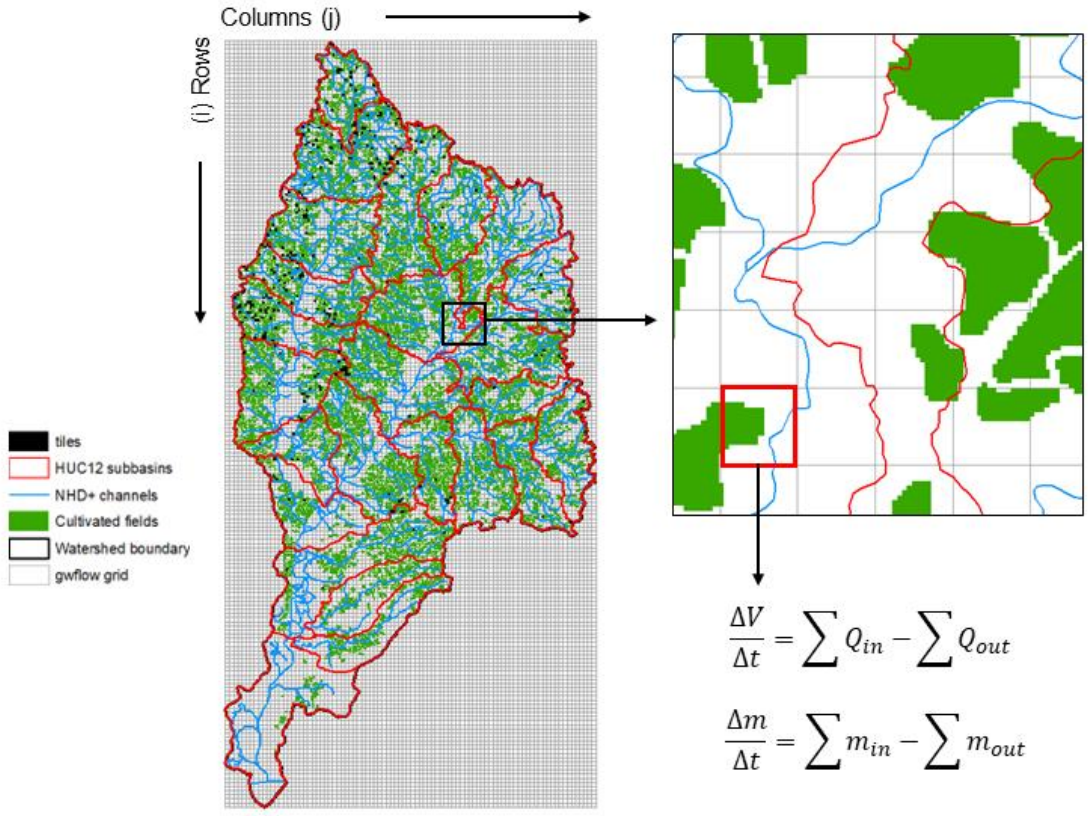

Figure 3: Spatial representation of gwflow grid within the context of SWAT+ objects (channels, subbasins, water bodies, fields), showing groundwater volume V and nitrate mass m mass balance equations used to update V and m for each grid cell for each time step of the simulation.

2.2.3 Including nitrate fate and transport in the gwflow module

To achieve the aims of this study, we amended the *gwflow* module code to simulate the mass storage, concentration, and transport of nitrate in the unconfined aquifer system, using the same grid cell setup as for the groundwater calculations (Equation 1). Mass and concentration are calculated for each grid cell, for each daily time step of the simulation, based on advection *adv*, dispersion *disp*, chemical reactions *rct*, and mass *sources* and *sinks*. Advection of nitrate mass is computed from groundwater inflows and outflows from/to neighboring cells. Dispersion is computed based on concentration gradients between adjacent cells. Nitrate mass sources for grid cells include recharge (leaching) from the soil profile, using recharge rates and leaching concentrations from the soil profile of spatially connected HRUs; and seepage from channels and reservoirs that are spatially connected to grid cells. Nitrate mass sinks include groundwater discharge to channels and reservoirs, pumping for agricultural irrigation for connected HRUs, and tile drainage outflow if tiles are in the grid cells. The only chemical reaction in groundwater included for nitrate is first-order denitrification.

For a single grid cell, the change in NO_3 mass m (g) over a given time Δt is calculated using the following mass balance equation:

$$\frac{\Delta m}{\Delta t} = adv_{in} - adv_{out} + disp_{in} - disp_{out} + \sum sources - \sum sinks - rct \qquad (2)$$

where adv_{in} (g) is the product of any groundwater flow rate (m^3) and nitrate concentration (g/m^3) from neighboring cells; adv_{out} (g) is the product of groundwater outflow and the cell's nitrate concentration (g/m3); $disp_{in}$ (g) is the dispersive mass transport into the cell, $disp_{out}$ (g) is the dispersive mass transport out of the cell; *sources* (g) are the product of flow rate (m^3) and nitrate concentration (g) of the groundwater inflow (recharge, seepage from channels, seepage from reservoirs); *sinks* (g) are the product of groundwater outflow from the cell (m^3) (groundwater discharge to channels and reservoirs, pumping for agricultural irrigation, and tile drainage outflow) and the cells NO_3 concentration (g); and *rct* (g) is the mass denitrified. Dispersion terms for the cell *i*,*j* are calculated as:

$$disp = \lambda \cdot \left(\frac{C_{NO_3(adj)} - C_{NO_3(i,j)}}{dist} \right) \cdot s_{avg} \qquad (3)$$

where λ is aquifer longitudinal dispersivity (m); *adj* signifies an adjacent cell; *dist* is the distance between centroid of cell *i*,*j* and the centroid of the adjacent cell (m); and s_{avg} is the groundwater saturated thickness (m) at the interface between cell *i*,*j* and the adjacent cell. For each cell *i*,*j*, dispersion is calculated for each of the four neighboring cells. If nitrate concentration in the neighboring cell is higher than the cell's concentration, then the mass is added to $disp_{in}$;

and vice versa for $disp_{out}$. The transport time step Δt is specified by the user as equal to or a fraction of the flow time step. The mass m of a cell for time $w+1$ is then updated in an explicit manner, using mass terms from time w:

$$m_{i,j}^{(w+1)} = m_{i,j}^{(w)} + \left(adv_{in} - adv_{out} + disp_{in} - disp_{out} + \sum sources - \sum sinks - rct\right)\left(t^{(w+1)} - t^{(w)}\right) \quad (4)$$

The cell's NO_3 concentration (g/m^3) is then updated using the groundwater volume (m^3) in the cell:

$$C_{NO_3 i,j}{}^{(w+1)} = \frac{m_{i,j}^{(w+1)}}{V_{i,j}^{(w+1)}} \quad (5)$$

If a fraction is specified, then V in Equation (5) is found by interpolating between groundwater volumes at the previous (n) and current ($n+1$) flow times (see Equation 1), and Equations 4 and 5 are repeated until the end of the flow time step has been reached. Due to the explicit method of updating cell mass, each cell must be provided with an initial mass (g) at the beginning of the simulation. To use this new feature of the *gwflow* module, the following inputs are required: initial nitrate concentration for each grid cell; longitudinal dispersivity, first-order denitrification rate, and the number of transport time steps for each flow time step.

At the end of each daily time step, the groundwater nitrate mass balance is computed by comparing, for the entire grid, the change in nitrate mass with the summation of mass from advection, dispersion, sources, sinks, and chemical reactions. Watershed-wide mass balance error, groundwater nitrate mass (kg), and mass flux (kg) for each mass balance component are written to files on a daily and annual basis. For annual, cell-by-cell values are written to file, to enable the creation of flux maps.

2.2.4 SWAT+ model for the Nanticoke River Watershed

Base SWAT+ model

For this study we created a SWAT+ model for the Nanticoke River Watershed, and then modified inputs to include the *gwflow* module. We then provided inputs for nitrate mass transport. The SWAT+ model is part of the National Agroecosystem Model (NAM) for CONUS, a nation-wide modeling effort to assess effects of conservation policies and environmental planning and hydrology, water quality, and sediment transport (Arnold et al., 2021; White et al., 2022). Within the NAM framework, individual SWAT+ models are developed for each of the 2,121 HUC8 (8-digit hydrologic unit code) watersheds within the CONUS. These models operate across five distinctive hydrologic and management domains: field (1–50 ha), transition (0.2–2.0 km²), headwater (1–15 km²), tributaries (15–150 km²), and main river (>150 km²). More information can be found at (Arnold et al., 2021). The dataset for constructing the based model is shown in **Table 2**. Detailed information on the construction of the SWAT+ model can be found in

(White et al., 2022). The Nanticoke River watershed is a headwater catchment; therefore, it does not receive flow from other upstream watersheds. For nitrate transport, a suite of soil, channel, and crop parameters are provided in input files, in addition to mineral and organic fertilizer rates.

Table 2: Dataset used for construction of the SWAT+ model.

Dataset	**Source**	**Resolution**
Watershed boundary	(USGS and USDA/NRCS 2013)	
Cropland field boundaries	(Yan & Roy, 2016)	
Digital Elevation Model	USGS National Elevation Dataset (Gesch et al., 2018)	10m
Soil Data	gSSURGO (Soil Survey Stat 2014)	10 m
Crop rotation	USDA-NASS, CDL	
Weather	Global Historical Climatology Network, PRISM	
Land use/cover	NLCD, USGS	30m
Streams and Rivers	National Hydrography Dataset Plus Version 2 (Moore & Dewald, 2016)	
Lakes and Reservoirs	National Hydrography Dataset Plus Version 2 (Moore & Dewald, 2016)	
Water Use	(Dieter et al., 2018)	
Discharge from facilities	National Permit Discharge Elimination System (Skinner & Maupin, 2019)	

Amending the SWAT+ model to include the gwflow module.

To implement the *gwflow* module into the base SWAT+ model, we use the datasets (geologic units, tile drainage locations, aquifer thickness, groundwater head) listed in **Table 3**. We employed a cell size of 500 m, resulting in a cell spatial area of 0.25 km^2. Ground surface elevation (m) for each grid cell is shown in **Figure 4**A; aquifer thickness (ground surface to bedrock, m) for each grid cell is shown in **Figure 4**B; geologic units (alluvial, fine detrital) are shown in **Figure 4**C; locations of tile drains are shown in **Figure 4**D. and initial groundwater head (m) for each grid cell is shown in **Figure 4**E. **Figure 4**E also shows the location of USGS monitoring wells, which provided the groundwater head data to perform the spatial interpolation.

Table 3: Dataset used for gwflow module input.

Dataset	**Source**	**Resolution**
Geological units	(Horton, 2017)	Vector Polygon
Tile Drainage	(Valayamkunnath et al., 2020)	30
Aquifer Thickness	(Shangguan et al., 2017)	250
Groundwater Head	(R. Bailey, 2022)	Vector points.

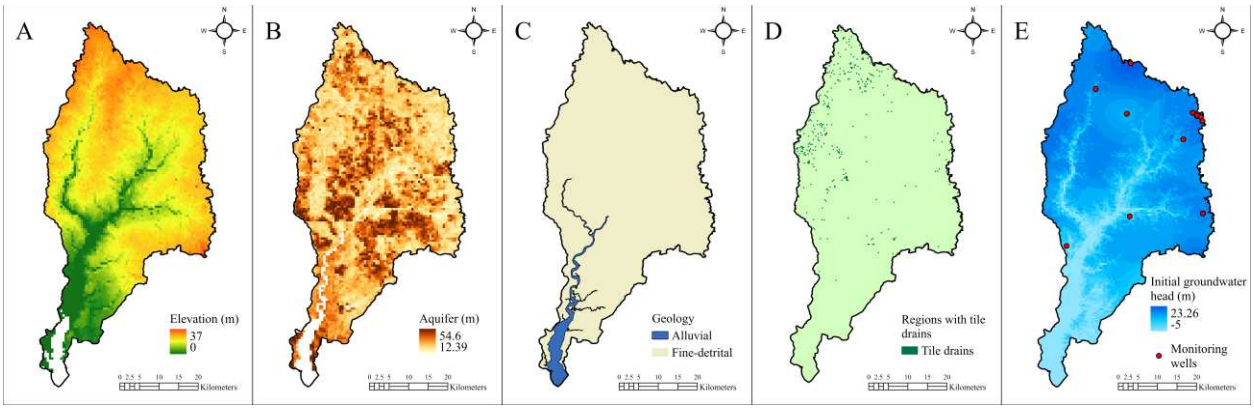

Figure 4: Maps showing (A) Ground Surface Elevation (m), (B) Aquifer Thickness (m), (C) Geologic units of the Nanticoke River Basin, (D) Tile drainage, and (E) Initial groundwater head and groundwater monitoring wells.

For NO_3 transport with the *gwflow* module, default values of denitrification rate (-0.0001 1/day) and longitudinal dispersivity (5 m) are specified. The transport time step is set to 1 day, to match the groundwater flow time step and the general time step of the SWAT+ simulation.

2.2.5 Model Calibration and Testing

The parameter estimation software (PEST) (Doherty et al., 2010) was utilized for calibrating and testing the SWAT+ model. PEST is a nonlinear, model-independent parameter estimator and uses local optimization technique to minimize user define objective function. The monthly streamflow of the SWAT+ model was evaluated at two stream gage locations (Bridgeville USGS 01487000; Adamsville USGS 01488500) based on Nash-Sutcliffe efficiency (NSE), percentage bias (PBIAS) and Kling-Gupta efficiency (KGE). The mean absolute error (MAE) is used to evaluate performance of the groundwater level at the available USGS monitoring wells (see **Figure 4**E for locations). The warmup period, calibration period, and testing periods are 2000-2001, 2002-2008, and 2009-2015, respectively. The monthly in-stream nitrate load (kg/month) of the SWAT+ model was evaluated at the Bridgeville site with 2012-2013 data from Ullman et al., (2013). The monthly loadings were calibrated from August 2012 to June 2013 and tested from July 2013 to May 2014.

The 16 parameters included in calibration are listed in **Table 4**: curve number, percolation, plant uptake compensation factor, soil evaporation compensation factor, initial water table depth, groundwater recharge delay, hydraulic conductivity of aquifer and streambed, streambed thickness, streambed depth, specific yield of the aquifer,

NO_3 percolation coefficient, and denitrification first-order rate constant. The table shows the initial (default) values, the lower and upper limits, and then the final (Estimated) calibrated value.

Table 4: Calibrated values for SWAT+ gwflow model.

Parameter	Estimated value	Initial value	Lower limit	Upper limit
Recharge delay (days)	**1.73**	2.00	1.00	30.00
Aquifer hydraulic conductivity (Alluvial)	**0.01**	0.01	0.00	0.10
Aquifer hydraulic conductivity (Fine-detrital)	**259.07**	500.00	50.00	1000.00
Aquifer specific yield (Alluvial)	**0.05**	0.05	0.04	0.35
Aquifer specific yield (Fine-detrital)	**0.35**	0.30	0.05	0.35
Streambed hydraulic conductivity (m/day)	**0.00**	0.01	0.00	1.00
Streambed thickness (m)	**2.00**	1.00	0.20	2.00
River depth (m)	**5.00**	5.00	1.00	10.00
Curve number	**40.00**	72.06	71.94	81.66
Soil evaporation compensation factor	**0.01**	0.08	0.01	1.00
Plant uptake compensation factor	**0.15**	1.00	0.10	1.00
Percolation coefficient (Alluvial)	**0.09**	0.10	0.09	1.00
Percolation coefficient (Fine-detrital)	**0.10**	0.90	0.10	1.00
Available water capacity	**0.39**	0.26	0.01	1.00
Nitrate percolation coefficient	**0.07**	0.10	0.01	1.00
Denitrification rate coefficient (1/day)	**1.00**	1.40	0.00	3.00

Quantifying the impact of climate change and land use on nutrient dynamics

The future climate projection data were taken from Multivariate Adaptive Constructed Analog (MACA) Climatology lab. The Multivariate Adaptive Constructed Analogs (MACA) is a statistical technique that enhances the resolution of Global Climate Models (GCMs) by transforming them from a course (several 100 km) to finer resolution (4 km) (http://www.climatologylab.org/maca.html). This process helps replicate the actual daily weather patterns and predicted alterations in GCM experiments at a finer scale. Two scenarios were selected: Representative Concentration Pathways (RCP) 4.5 and 8.5. RCP 4.5 predicts a future where emissions peak around 2040s and then decline due to moderate mitigation efforts and cleaner technologies. This scenario reflects a world taking measures to curb climate change. In contrast, RCP 8.5 depicts a high emissions future driven by fossil fuel use and limited mitigation, representing a "business-as-usual" approach. Three models (MIROC5, GFDL-ESM2M, and IPSL-CM5A-LR) (Table 5) were selected based on studies performed by Delaware Climate Change Impact Assessment. Other models were not chosen due to inaccurate replication of historical data. For example, the CCSM4 and IPSL-CM5A models tend to overestimate observed maximum temperature trends, while the CNRM-CM5, HadGEM2 and INMCM4 models tend to underestimate the maximum temperature trends. Using an ensemble of these three models for climate change projections best captured the trend in observed data.

To implement the climate data from these 3 models into the SWAT+ simulations, the climate data was downloaded for each of the 25 subbasins of the watershed, using the subbasin centroid. These data were then input for each day of the 2024-2099 period, and the model simulation period was set to 2024-2099.

Table 5: CMIP5 Model Description.

CMIP5 Model	**Description**
GFDL-ESM2M	National Oceanic and Atmospheric Administration (NOAA), Geophysical Fluid Dynamics Laboratory Earth System
MIROC-ESM	Japan Agency for Marine-Earth Science and Technology, Atmosphere and Ocean Research Institute (The University of Tokyo)
IPSL-CM5A-LR	Institute Pierre Simon Laplace Climate Model 5A, Low-Resolution

The predicted precipitation and temperature for the 2024-2099 period, using the average of the 3 models, are shown in **Figure 5**. The baseline average annual rainfall, T_{max}, and T_{min} are 1155.1mm, 19.66° and 8.04°. All climate variables increased for all future timelines under RCP 4.5 and RCP 8.5 scenarios. The absolute ensemble changes in average annual maximum temperature are 1.87°, 2.61°, and 3.16° under RCP 4.5 and 2.11, 3.74, and 5.44 under RCP 8.5 scenarios for near, mid, and far future timelines. Similarly, the absolute ensemble changes in average annual minimum temperature are 1.83°, 2.61°, and 3.12° under RCP 4.5 and 2.07°, 3.67°, and 5.46° under RCP 8.5 scenarios for near, mid, and far future timelines. Under RCP 4.5, we expect a modest 3-8% increase in precipitation, a 10-16% rise in maximum temperature, and a 23-39% increase in minimum temperature compared to baseline annual averages. Under RCP 8.5, the changes are more pronounced, with a 3-7% increase in precipitation, an 11-28% rise in maximum temperature, and a more significant 26-68% increase in minimum temperature compared to baseline annual averages. The annual precipitation of the watershed is expected to increase very slightly for both scenarios. The projected climate variables are seen in **Figure 5**. This trend is similar to studies conducted by (Modi et al., 2021;Najjar et al., 2010;Seong & Sridhar, 2017), with the Chesapeake Bay region generally projected to experience increases in air temperature and precipitation amount and intensity over the next century.

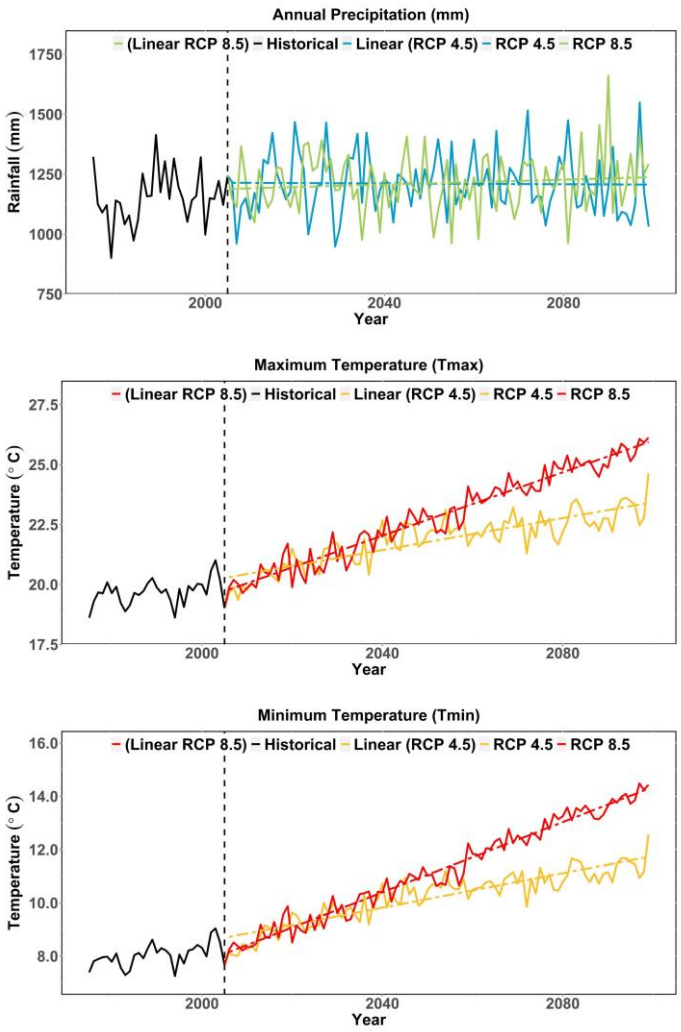

Figure 5: Projections of ensemble climate model for future precipitation, maximum temperature and minimum temperatures under RCP 4.5 and RCP 8.5 Scenario for entire future timeline.

For the future land use scenario, a projected 250 m resolution land use for the Conterminous United States Land Cover Projections spanning from 1992 to 2100 has been used (Sohl, 2018). The scenario used in this study is an environmentally focused scenario which shows decline in agricultural land (i.e., transfer to urban land use). Using historical patterns from 1992-2005 using the National Land Cover Database (NLCD), USGS Land Cover Trends, and US Department of Agriculture's Census of Agriculture, projections were made for the 2006-2100 period. The land use projection used in this study is based on a scenario that envisions a world where the primary emphasis is placed on finding environmentally sustainable solutions at the local and regional levels for the future. In this scenario, there is a balance between population growth, moderate economic development, and a slower, more diverse pace of technological advancement. While environmental protection and social equity remain important, the central focus is

on fostering sustainability within local and regional contexts. The % of cropland converted to other land use is reported in **Table 6**. Future maps of 2036, 2061, and 2086 have been used for the near, mid, and future periods, respectively. The projected maps were then overlapped with the HRUs in the watershed, with the predominant land use chosen as the focal point for the alteration in land use.

Table 6: % of cropland changed to other land use.

% Cropland converted to	**Near Future**	**Mid Future**	**Far Future**
Forest	22%	17%	17%
Hay	15%	17%	19%
Wetland	4%	2%	2%
Urban	3%	3%	2%
Rangeland	0%	0%	0%
Pasture	1%	1%	1%
Barren	1%	1%	1%

For each scenario, model results are analyzed for system-response variables (groundwater head, groundwater nitrate concentration, streamflow, in-stream nitrate loads), response fluxes (hydrologic, nutrient) on the land surface, in soil profiles, and in the unconfined aquifer system. The fluxes influencing the streamflow and nitrate loading are analyzed for seasonal variation and average annual hydrological fluxes in comparison to historical values.

CHAPTER 3- RESULTS AND DISCUSSION

3.1 Historical Hydrology

Simulated and observed streamflow for the two gage locations are shown in **Figure 6**, demonstrating quick responses to precipitation and periods of low flow and high flow. The model is able to capture the rise and recession of streamflow, and the baseflow patterns. The ability of the model to capture baseflow patterns is a reflection on the use of the physically based manner in which the *gwflow* module is constructed to simulate groundwater flow and groundwater-channel interactions. NSE values are 0.79 and 0.72, respectively, for the two gages for the calibration period, and 0.86 and 0.77 for the testing period. PBIAS is small, indicating neither strong underestimation nor overestimation by the model. The mean absolute error for 26 monitoring wells with 173 data points is 1.11 m for the monitoring stations in the Nanticoke watershed.

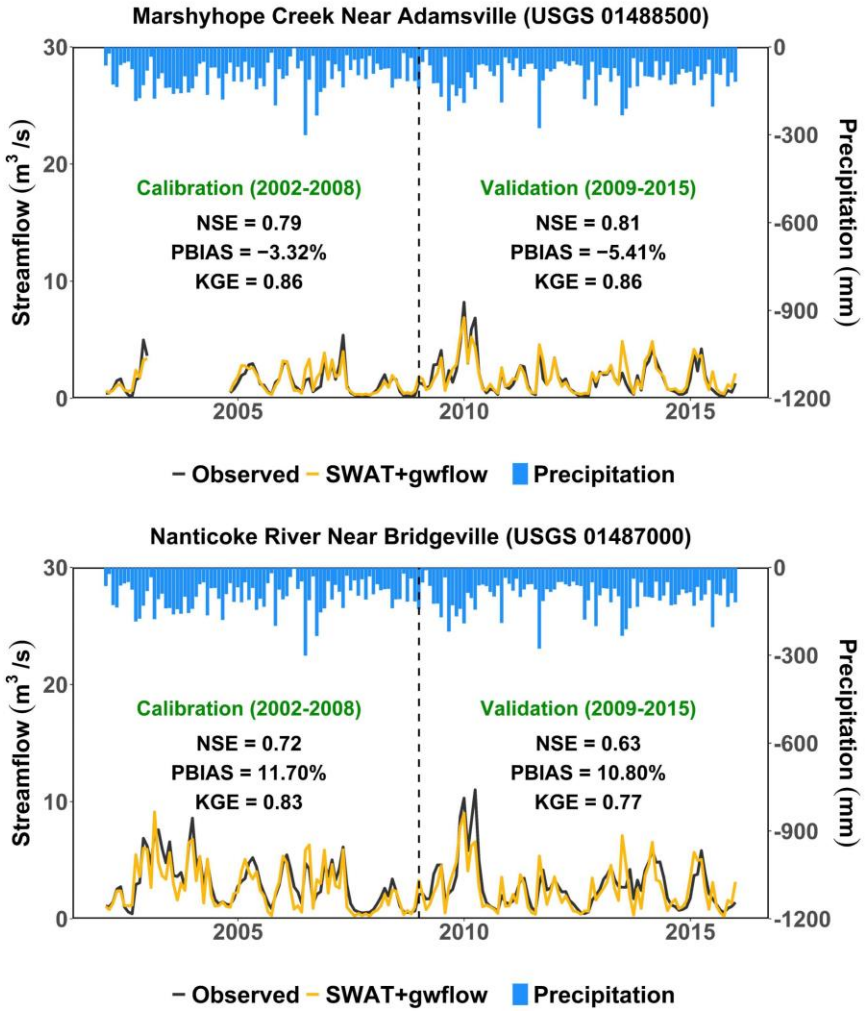

Figure 6: Observed vs simulated monthly streamflow during calibration and validation at two stations.

Streamflow is composed of surface runoff, soil lateral flow, groundwater saturation excess flow, and tile drainage outflow. Of the generated streamflow (588 mm/yr), 40% is from surface runoff, 21% is from soil lateral flow, 37.5% is from groundwater saturation excess flow, and 0.5% is from tile drainage outflow. Therefore, the baseflow fraction, i.e., the contribution of subsurface flow (soil lateral flow, groundwater discharge) to streamflow, is 59%, indicating the strong connection between the unconfined aquifer and the channel network. The monthly fluxes (mm) for each hydrologic component are shown in **Figure 7** for the watershed system (A) and the aquifer system (B), demonstrating the seasonal nature of fluxes such as precipitation, ET, recharge, groundwater pumping for agriculture, and saturation excess flow. Spatial representations (cells: 500 m resolution) of recharge and saturation excess flow (for the year 2015) are shown in **Figure 8**, along with average groundwater head (m) and water table depth (m).

Table 7: Average annual hydrologic fluxes (mm).

Flux	**mm/yr**
Precipitation	1181
Boundary Inflow	139
ET	800
Surface Runoff	238
Soil Lateral Flow	126
Stream seepage	0
Sat Excess Flow	221
Tile flow	3
Recharge	32
Pumping Irrigation	15
GW-Lake Exchange	1
Surface Water Irrigation	1
Water Yield	588

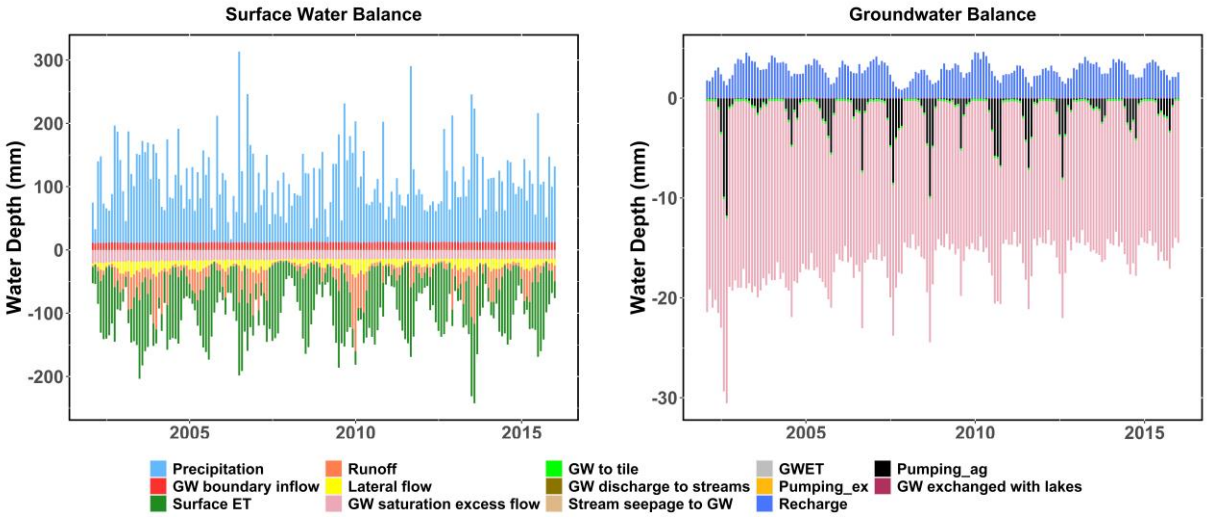

Figure 7: (A) Monthly surface water fluxes (mm) (B) Monthly groundwater fluxes for the simulation period (2000-2015).

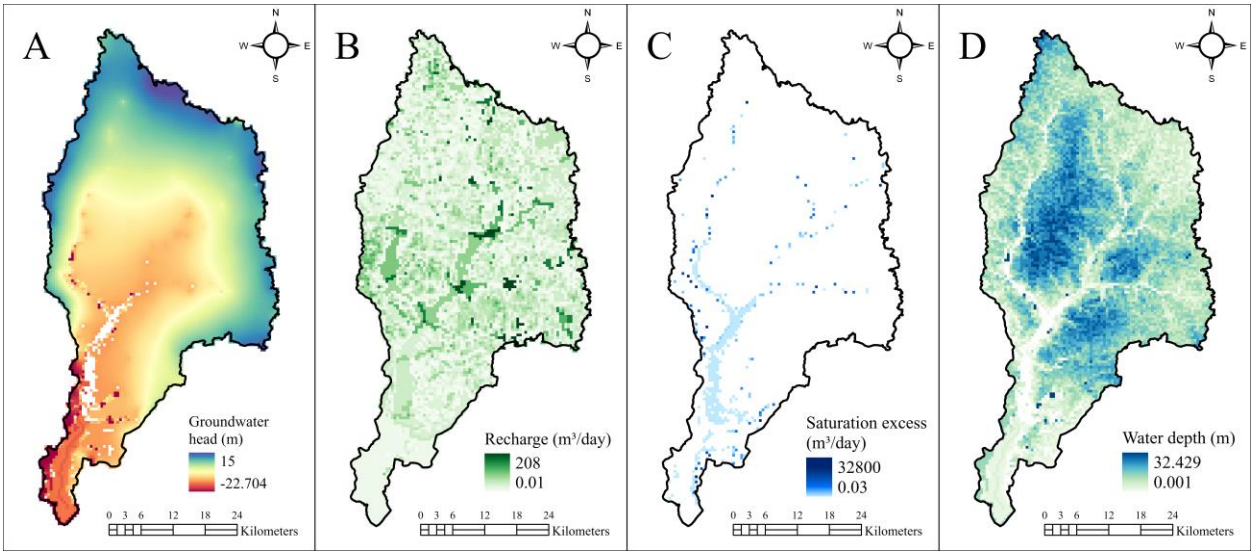

Figure 8: Map of (A) groundwater head; (B) recharge; (C) saturation excess flow; (D) water depth for the year 2015.

3.2 Historical Nutrient Fate and Transport

Simulated and observed monthly in-stream nitrate load (kg) for the Bridgeville gage is shown in **Figure 9**, demonstrating a good agreement (NSE = 0.76, 0.61) for the calibration and testing periods. Particularly, the model captures the increase in loadings during the spring and early summer months. Of the watershed loadings that contribute to in-stream loading (**Table 8**, "Channel system"), 46% is from surface runoff, 33% is from soil lateral flow, and 21% is from groundwater saturation excess flow. Note that the nitrate contribution of soil lateral flow (33%) is higher than the streamflow contribution (21%), whereas the nitrate contribution of groundwater saturation excess flow (21%) is

much lower than the streamflow contribution (37.5%). This is due to nitrate concentrations in soil water being higher than nitrate concentrations in groundwater. The overall nitrate mass loading for each system type (soil, aquifer, channel) is shown in Table 8, with positive values indicating a system input and negative values indicating a system output. For the aquifer system, of note is that nitrate mass lost via denitrification (440,000 kg) is on par in magnitude with the nitrate mass lost via saturation excess flow (640,000 kg). To provide understanding of the spatial variation in system responses and fluxes, simulated groundwater nitrate concentration, recharge (leaching) mass, and saturation excess flow mass is shown in **Figure 10** for the year 2015.

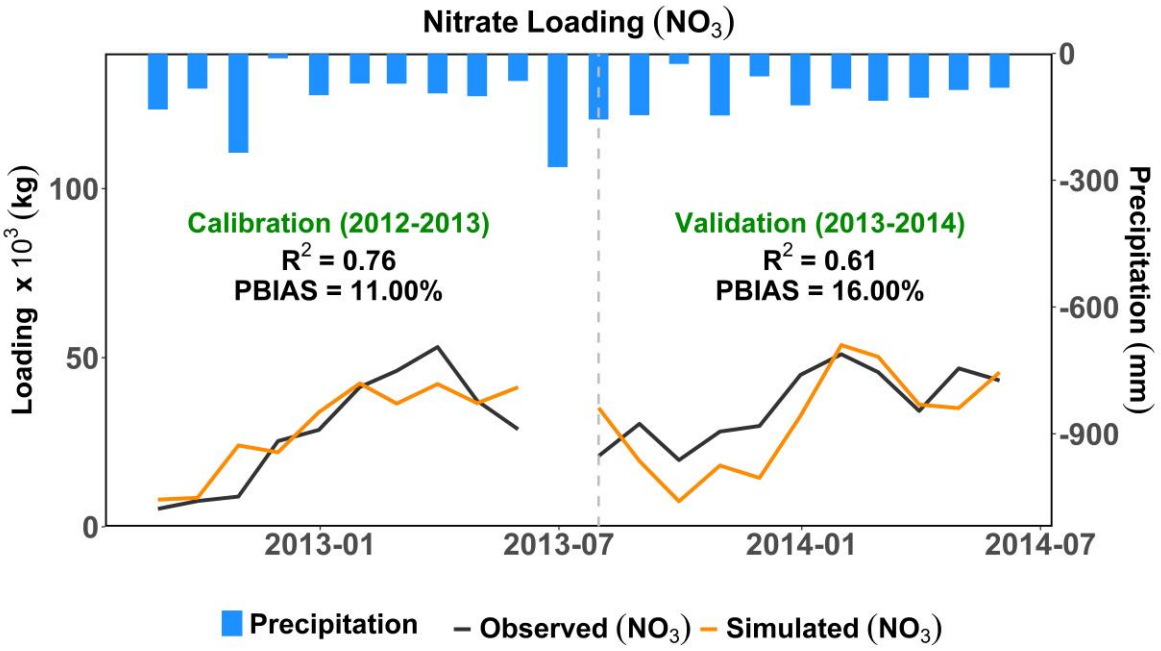

Figure 9: Observed and simulated monthly nitrate loading at Bridgeville station.

Table 8: Annual average nitrate fluxes for all systems.

Nitrate (kg) in Soil system	
Atmospheric deposition	1256512
Nitrification	23992860
Residue decomposition	28982428
Organic N mineralization	23992860
Plant Uptake	-16951448
Soil denitrification	-548209
Surface runoff	-1446757
Soil Lateral flow	-1012894
Soil tile flow	0
Leaching to water table	-1269336
Groundwater transfer to soil	0
Nitrate (kg) in Groundwater system	

Leaching to water table	1269336
Groundwater transfer to soil	0
Groundwater denitrification	-440004
Groundwater tile flow	-11231
Discharge to streams	-2451
Saturation excess flow	-640389
Pumping irrigation	-32960
Pumping specified	0
Seepage streams	1057
Seepage canals	0
Seepage lakes	800
Seepage floodplains	0
Nitrate (kg) in Channel system	
Surface runoff	1446757
Soil Lateral flow	1012894
Soil tile flow	0
Groundwater tile flow	11231
Discharge to streams	2451
Saturation excess flow	640389
Seepage to streams	-1057

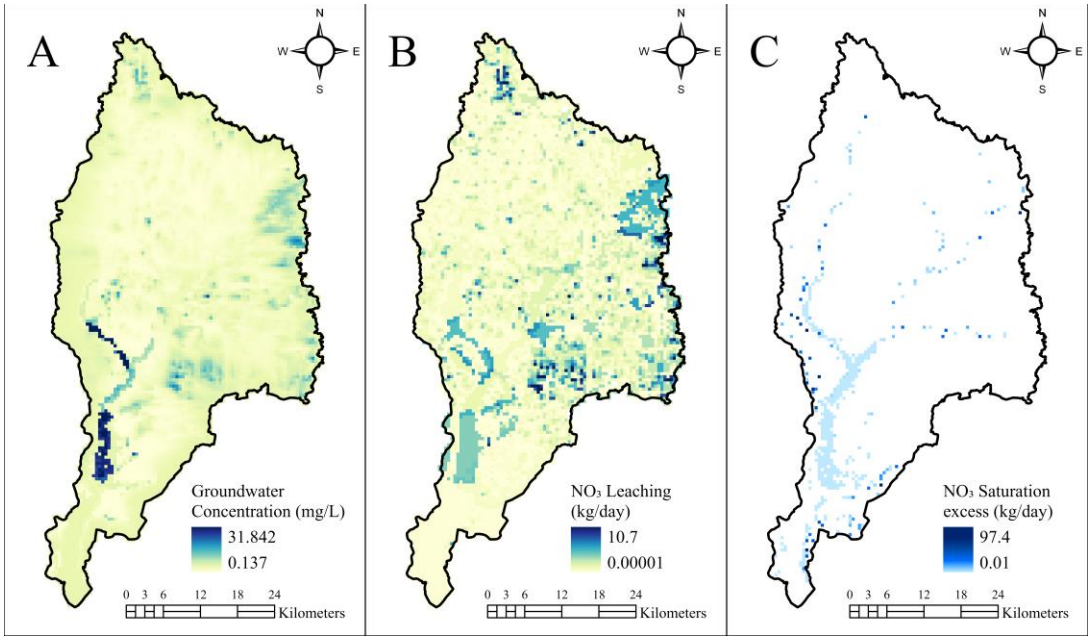

Figure 10: Maps showing (A) groundwater concentration; (B) nitrate leaching; (C) nitrate from saturated excess flow for the year 2015.

3.3 Future Nutrient Fate and Transport

3.3.1 Changes in Streamflow

Under RCP 4.5, the annual average precipitation was projected to increase 5% for the near future, 8% for mid future and 3% for far future. Using the SWAT+ model for future periods, the projected decrease in annual average

streamflow for the same timelines was 22%, 18% and 34%, respectively as compared to the baseline historical period of 2000-2015. Under RCP 8.5, future streamflow during these three periods is 22%, 33%, and 30%. **Figure 11** shows average monthly flows (January through December) for the baseline model, the RCP4.5 models, and the RCP8.5 models, indicating that flows from summer through early winter are projected to decline whereas there is an increase seen in early spring flow in the Nanticoke River watershed.

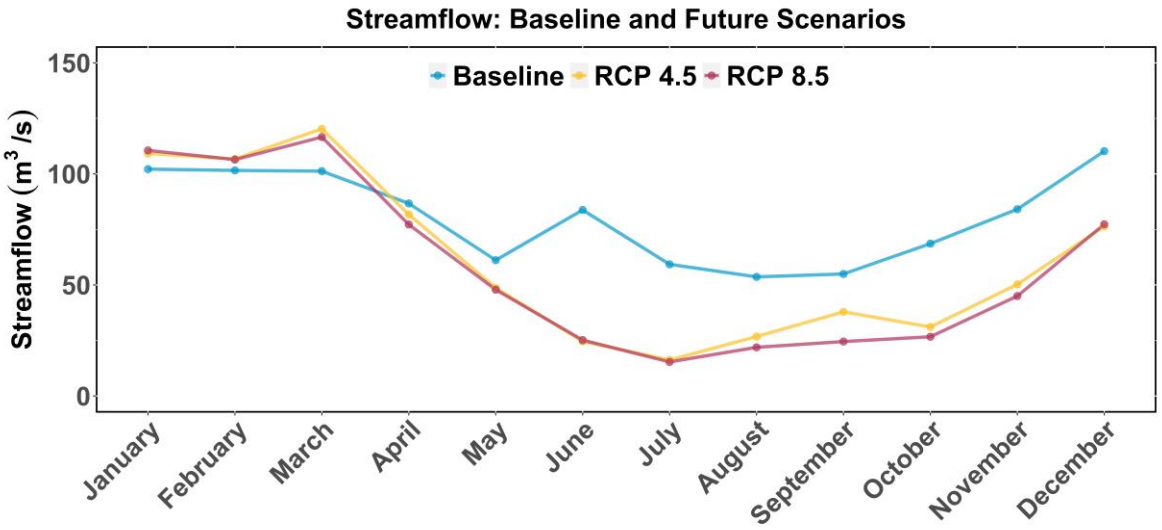

Figure 11: Temporal variation in streamflow of RCP 4.5 and 8.5 scenarios as compared to the baseline.

The streamflow peaks during the month of March for both future climate scenarios. A 19% and 15% increment from baseline streamflow is seen during the month of March for RCP 4.5 and RCP 8.5 respectively, influenced by higher precipitation and lower evapotranspiration rates as seen in **Table 9** and **Figure 12**. The spring season has an increase in the seasonal average precipitation as compared to baseline of 6% and 7% for RCP 4.5 and RCP 8.5 respectively. The seasonal average evapotranspiration decreased by 2% and 1% as for both climate scenarios with a reduction in the evapotranspiration which leads to the peak in the month of March. In contrast to the peak in March, a significant decrease of 73% and 74% from baseline streamflow is seen during the month of July for RCP 4.5 and RCP 8.5, respectively. This decrease is due to lower precipitation and higher evapotranspiration rates. The summer season has a decrease in the seasonal average precipitation of 8% and 10%, and an increase of seasonal average evapotranspiration by 12% and 11% for RCP 4.5 and RCP 8.5 respectively. The peak in the month of September for RCP 4.5 (121.31 mm) is due to a higher average precipitation flux as compared to RCP 8.5 (113.5 mm). The overall

decline in monthly streamflow is due to higher temperatures resulting in higher evapotranspiration, offsetting the additional precipitation. These results are in agreement with previous watershed modeling studies conducted in the Chesapeake Bay region, predicting increases in spring streamflow coupled with decreases in summer streamflow as a result of climate change (Alamdari et al., 2017; Du et al., 2018; Hawkins, 2015; Mukundan et al., 2020; Wagena et al., 2018)

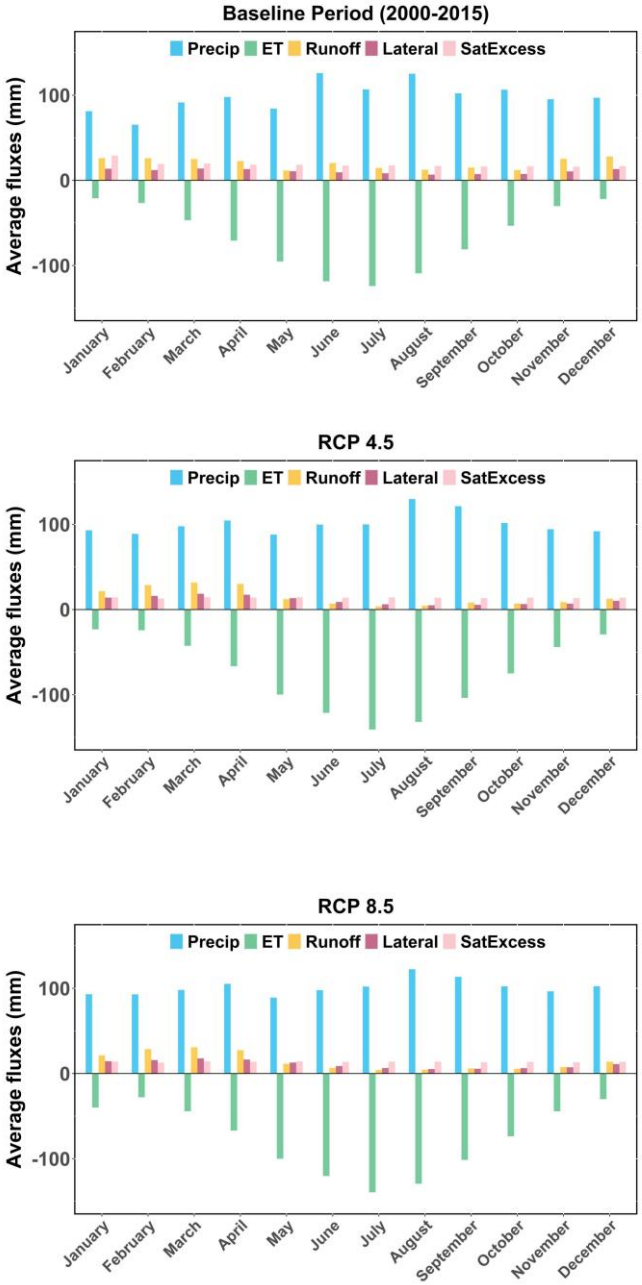

Figure 12: Average hydrological fluxes for channel system (A) Baseline; (B) RCP 4.5; (C) RCP 8.5

Table 9: Percentage Change in average fluxes between baseline and future scenarios for four seasons.

Seasons	RCP 4.5		
	% Change Precipitation	**% Change Evapotranspiration**	**% Change Runoff**
Winter (Dec, Jan, Feb)	12%	10%	-21%
Spring (March, April, May)	6%	-2%	26%
Summer (June, July, August)	-8%	12%	-68%
Fall (September, October, November)	4%	35%	-55%
	RCP 8.5		
Winter (Dec, Jan, Feb)	19%	41%	-20%
Spring (March, April, May)	7%	-1%	18%
Summer (June, July, August)	-10%	11%	-68%
Fall (September, October, November)	3%	33%	-64%

3.3.2 Changes in in-stream nitrate loading

Figure 13 shows the average annual nitrate loading for all future timelines under RCP 4.5 and RCP 8.5. The changes in average annual are in response to projected climate change based on ensemble GCM CMIP5 predictions. For each timeline under both scenarios, **Table 10** depicts the changes in the annual average loading as compared to the baseline.

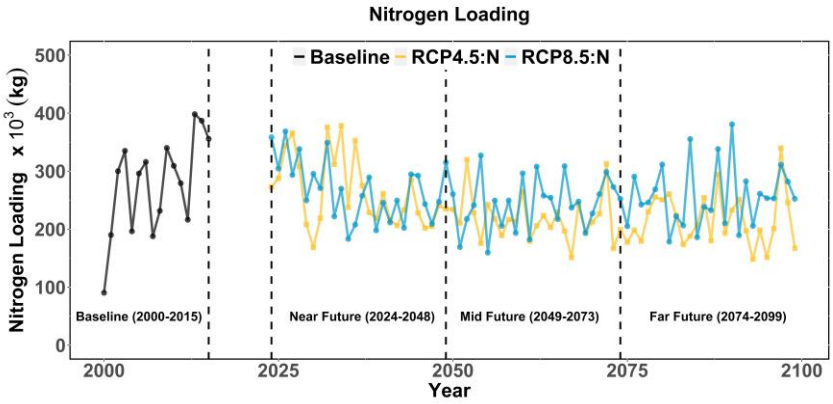

Figure 13: Future Nitrogen Loading for both scenarios and baseline.

Table 10: % Change of Nitrate loading compared to baseline period.

Timeline	RCP 4.5	RCP 8.5
2024- 2048 (Near Future)	-4%	-4%
2059 -2073 (Mid Future)	-21%	-11%
2074-2099 (Far Future)	-22%	-8%

The results indicate a shift in the temporal scale, with the nitrate loads peaking during May. A decline in nitrate loads is projected in the summer months compared to the baseline loading for both scenarios as seen in **Figure**

14. This decrease in nutrient loading in the summer months is due principally to a decrease in surface runoff (see Section 3.3.1), resulting from higher ET rates. These results are similar to those of Kalcic et al. (2019) in their study of climate change impacts on nutrient loading in the Lake Erie basin, in which loading was decreased due to an increase in ET in a warmer climate, despite projected increases in precipitation. For our study, the maximum increment in average annual nitrate loading is projected to occur in May averaging about 10% and 15% more than baseline loading for RCP 4.5 and 8.5 respectively. March is the first month after summer which is expected to see higher nitrate loading as compared to baseline period, which matches the increased monthly streamflow pattern for both scenarios. During the month of March, there is an increment of 1% and 19% nitrate loading than baseline loading for RCP 4.5 and 8.5 respectively. Our results were not in agreement with the results of (Alamdari et al., 2020; Bhatt et al., 2023; Wagena et al., 2018) where the nitrate loadings are projected to increase for future climate scenarios. However, differences in these results may indeed be attributed to differences in climate model projections, where our models predict lower precipitation and higher temperatures compared to those utilized in the studies mentioned. Greater precipitation estimated in their study likely results in increased nitrate loading from runoff, further adding to the differences in the projected outcomes.

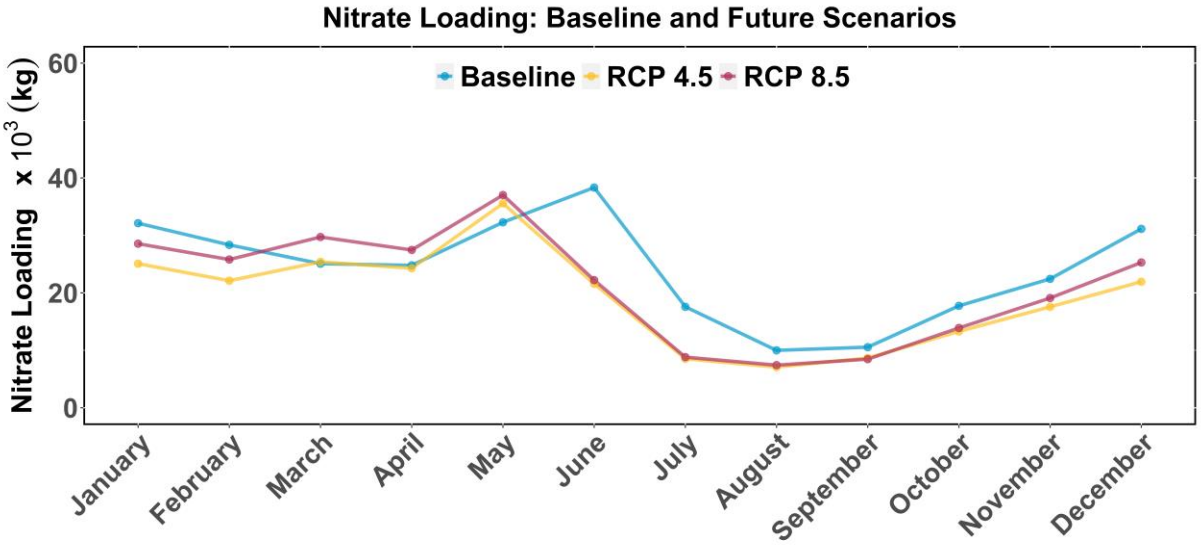

Figure 14: Temporal variation in Nitrate loading of RCP 4.5 and 8.5 scenarios as compared to the baseline.

Analyzing model results indicates a shift in the contributors of nitrate loading. During both future scenarios, the dominating element that contributes nitrate loading into the channel system changes from runoff to lateral flow and saturated excess flow, as seen in **Figure 15**. The contribution of average annual nitrate loading from runoff decreases by 41% and 38%, due to a decrease in surface runoff resulting from higher ET in the warmer climate, from lateral flow increases by 18% and 48% and finally the from saturated excess flow increases by 102% and 109% respectively for the entire period of RCP 4.5 and RCP 8.5 as compared to the baseline. Changes in seasonal values are shown in **Table 11**. Since the amount of nitrate-nitrogen is estimated as a product of volume of water and average concentration of nitrate, the increment in nitrate loading coming from lateral flow and saturated excess flow is attributed to higher concentration of nitrate in the soil and groundwater system.

Table 11: % of Annual average nitrate loading change for both climate scenarios with respect to baseline.

Seasons	**RCP 4.5**		
	% Change Runoff	**% Change Lateral**	**% Change Saturation excess**
Winter (Dec, Jan, Feb)	-52%	11%	93%
Spring (March, April, May)	-31%	49%	109%
Summer (June, July, August)	-37%	13%	106%
Fall (September, October, November)	-42%	-14%	100%
	RCP 8.5		
Winter (Dec, Jan, Feb)	-46%	51%	100%
Spring (March, April, May)	-26%	72%	116%
Summer (June, July, August)	-40%	34%	113%
Fall (September, October, November)	-38%	22%	107%

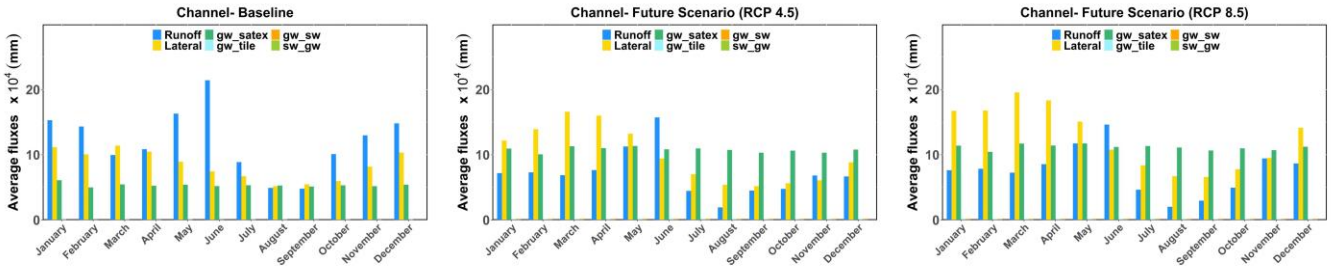

Figure 15: Temporal variation in nitrate fluxes in the channel system for baseline, RCP 4.5, and RCP 8.5.

Within the context of an increase in nitrate loading from soil lateral flow and groundwater saturation excess flow, we now consider the mechanisms that govern nitrogen in the soil system. Nitrogen is removed from the soil profile principally by plant uptake and leaching to the groundwater system. Within a warmer future climate,

mineralization decreases by 21% for RCP 4.5 and 19% for RCP 8.5 and water content also decreases, leading to nitrogen stress and consequent diminished nitrate uptake (28%, 32% decrease), resulting in an increase in leaching to groundwater. **Figure 16** shows the temporal variation in nitrate fluxes for the soil system.

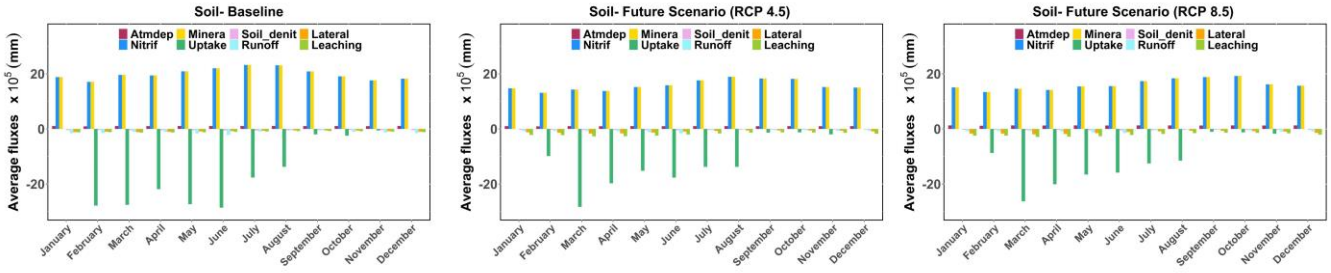

Figure 16: Temporal variation in nitrate fluxes in the soil system for baseline, RCP 4.5, and RCP 8.5.

Besides an impact on leaching, decreased nitrate uptake also has an influence on crop yield. There is a notable decrease in the crop yield for corn and soybean, the two main crops in the Nanticoke Watershed, as shown in **Table 13**. Increase in temperature results in higher water stress and negatively influences crop yield. This is corroborated by the fact that under RCP 4.5 and RCP 8.5, the crop yield decreased by 28% and 32% respectively. Similar results were reported by Paul et al., (2020) for a watershed in the Mid-Atlantic region, where a negative correlation exists between temperature and crop yields. Decrease in both corn and soybean yields were noted in RCPs in the late century, except in RCP 4.5, where soybean yields slightly increased which might be due to the combined impact of precipitation and temperature (Paul et al., 2020). For the Nanticoke River watershed, as compared to the RCP 8.5 scenario, RCP 4.5 does have a slightly higher projected precipitation that might explain the increase in crop yield for soybean for the RCP 4.5 scenario as reported in **Table 13**.

Table 12: % change of fluxes as compared to Baseline period.

Fluxes	**RCP 4.5**	**RCP 8.5**
Channel System		
Runoff	-41%	-38%
Lateral	18%	48%
Groundwater Saturation excess flow	102%	109%
Groundwater System		
Leaching	80%	98%
Soil System		
Plant uptake	-28%	-32%

Table 13: % change in crop yield for future scenarios as compared to baseline period.

Crop Type	RCP 4.5 Crop Yield (tons/ha)	RCP 8.5 Crop Yield (tons/ha)
Corn	-17%	-27%
Soybean	3%	-4%

Annual average nitrate leaching increases significantly, 80% for RCP 4.5 and 98% for RCP 8.5. This increase in nitrate leaching, without a similar rise in actual recharge volume, results in an increase in concentration of nitrate within the groundwater system, eventually resulting in an increased concentration and loading of nitrate when saturated excess flow enters the channel system. **Figure 17** shows the temporal variation in nitrate fluxes for the groundwater system.

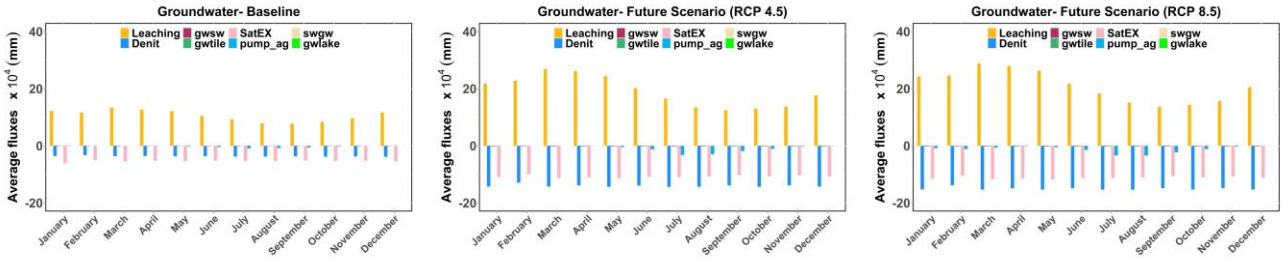

Figure 17: Temporal variation in nitrate fluxes in the groundwater system for baseline, RCP 4.5, and RCP 8.5.

3.4 Incorporating Land Use Change

From the results of the future simulations including land use change, nitrogen dynamics in the watershed is much more sensitive to climate change as compared to land use change. A decrease of 0.04-1.7% is reported for RCP 4.5 when land use is incorporated. Similarly, a decrease of 0.15-1.80 % is reported for RCP 8.5 when land use change is incorporated. in nitrate loading occurs due to the introduction of land use change scenario as seen in **Table 14** and can be visualized in **Figure 18** . The marginal reduction in nitrate loading resulting from the implementation of land use changes with an environmental focus may be attributed to the specific spatial arrangement. Gémesi et al., (2011) suggests that spatial arrangement of land types, not just their proportions in the watershed impact the water quality. Having forests near streams (riparian buffers) helps to limit the amount of nitrogen that goes from farmlands into the streams. However, even with these forests in place, if there's a lot of croplands around, it can still be the main reason why there's a lot of nitrogen going from the land into the streams in a specific area of the Chesapeake region (Liu et al., 2000; Weller et al., 2011; Weller & Baker, 2014).

Table 14: % change in annual average nitrate loading compared to only climate scenarios RCP4.5 and RCP8.5

Timeline	RCP 4.5 + Land use	RCP 8.5 + Land use
Near Future (2024-2048)	-1.70%	-1.80%
Mid Future (2049-2073)	-0.75%	-0.61%
Far Future (2074-2099)	-0.04%	-0.15%

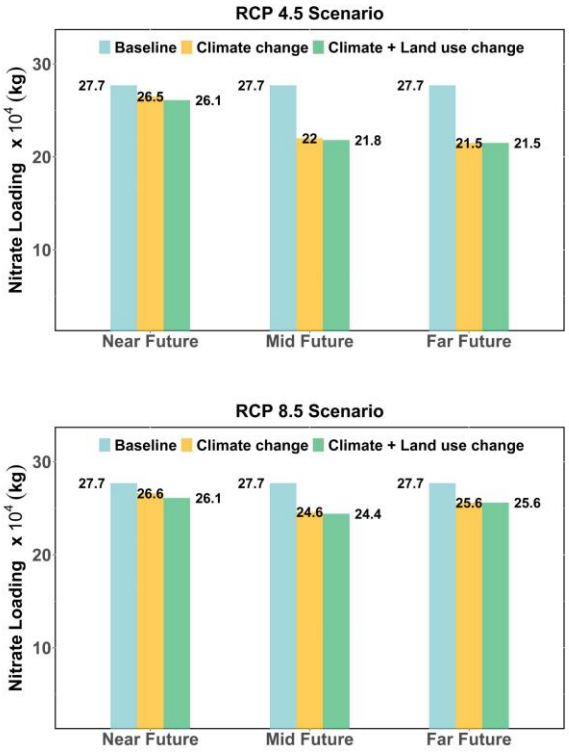

Figure 18: Comparing annual average nitrate loading for RCP 4.5 and 8.5 under CC and CC+LU.

3.5 Study Limitations

Although we have attempted to provide a holistic approach to modeling the fate and transport of nitrate in a complex watershed system under both historical and future conditions, there are of course limitations to our approach. These are:

a. *Limited in-stream loading nitrate data*. Ideally, we would be able to test the model at multiple gage sites, for an extended period (i.e., at least decadal). However, data are available only for one gage site (Bridgeville) for two years.

b. *Limited groundwater nitrate data*. Whereas there are many groundwater head data at monitoring well locations throughout the watershed, nitrate concentration data are sparse. More data would be helpful to test the simulated spatial distribution of groundwater nitrate concentration (see **Figure 11**).

c. *Groundwater saturation excess flow*. Under ideal conditions, shallow groundwater (i.e., within the soil profile) would be transferred from the aquifer to the soil profile, and then soil water balance equations would be used to simulate any saturation excess. However, in this model set-up, we have neglected this transfer and instead allowed groundwater, under wet conditions, to rise to the ground surface resulting in groundwater saturation excess flow. We believe this is acceptable for a regional scale application, such as with the Nanticoke River Watershed, and for a shallow unconfined aquifer in connection with channels. New updates to the *gwflow* module have allowed the transfer between aquifer and soil to occur (Yimer et al., 2023), and will be used in future nutrient studies.

CHAPTER 4- SUMMARY AND CONCLUSIONS

In this study we use the SWAT+ model, updated to simulate physically based spatially distribution nitrate transport in aquifer systems, to quantify the impact of climate change and land use change on surface-subsurface nutrient dynamics of the Nanticoke River Watershed, a tributary watershed to Chesapeake Bay. The future downscaled climate data was extracted from MACA climatology lab under two climates scenarios RCP 4.5 and RCP 8.5. The future land use maps were selected from USGS projections using the FORE-SCE model which was an environmentally focused scenario. From model results, we conclude the following:

a. Although climate change projects an increase in precipitation by 3-8% for RCP 4.5 and 3-7% for RCP 8.5, the streamflow in the Nanticoke River decreases by 18-34% and 20-33% for both scenarios, respectively, as compared to the baseline period of 2000-2015. This decrease is due to higher evapotranspiration rates during the summer months, within the projected warmer climate.
b. The nitrate loadings within the Nanticoke River during future periods decrease slightly during the summer months as compared to the baseline period of 2000-2015 under both RCP 4.5 and RCP 8.5 scenarios by 4-22% and 4-11% respectively. This is due mainly to a decrease in surface runoff, from an increase in overall ET. However, the decrease in runoff is offset somewhat by the increase in nitrate loading from groundwater saturation excess flow, due to an increase in groundwater nitrate concentrations, from higher nitrate leaching loads from the soil profile.
c. The nitrate loading contribution to the aquifer system via leaching is higher for future scenarios due to decreases in plant uptake from the soil system, which is a result from changes in nitrogen mineralization and water stress in a drier soil. A 28% and 32% reduction in plant uptake is seen in RCP 4.5 and RCP 8.5 scenarios respectively. This change in plant uptake, along with temperature stress due to rising temperatures, resulted in a decrease in corn and soybean yields in the watershed.
d. Under land use, the croplands were projected to change 15% to forest areas and 18% to hay. However, these changes had minimal impact on the nitrate loadings, as compared to the effect of climate change.

These insights can be used to assist with nutrient management in the Nanticoke River Watershed and other tributary watersheds to Chesapeake Bay. Furthermore, the updated SWAT+ model, with physically based nitrate fate and transport modeling in the aquifer system, provides a holistic modeling tool for investigating the impact of management strategies and system changes on nutrient dynamics in a watershed system. The updated SWAT+ model and code can be downloaded from the website https://swat.tamu.edu/software/plus/.

REFERENCES

Adams, J. B., Taljaard, S., van Niekerk, L., & Lemley, D. A. (2020). Nutrient enrichment as a threat to the ecological resilience and health of South African microtidal estuaries. *Afr. J. Aquat. Sci.*, *45*(1–2), 23–40. https://doi.org/10.2989/16085914.2019.1677212

Alamdari, N., Sample, D. J., Ross, A. C., & Easton, Z. M. (2020). Evaluating the Impact of Climate Change on Water Quality and Quantity in an Urban Watershed Using an Ensemble Approach. *Estuaries Coast.*, *43*(1), 56–72. https://doi.org/10.1007/s12237-019-00649-4

Alamdari, N., Sample, D. J., Steinberg, P., Ross, A. C., & Easton, Z. M. (2017). Assessing the effects of climate change on water quantity and quality in an urban watershed using a calibrated stormwater model. *Water*, *9*(7). https://doi.org/10.3390/w9070464

Arnold, J. G., White, M. J., Allen, P. M., Gassman, P. W., & Bieger, K. (2021). Conceptual Framework of Connectivity for a National Agroecosystem Model Based on Transport Processes and Management Practices. *J Am Water Resour Assoc*, *57*(1), 154–169. https://doi.org/10.1111/1752-1688.12890

Ator, S. W., Brakebill, J. W., & Blomquist, J. D. (2011). Sources, fate, and transport of nitrogen and phosphorus in the Chesapeake Bay watershed: an empirical model. In *USGS Scientific Investigations Report* (Vol. 5167).

Ator, S. W., García, A. M., Schwarz, G. E., Blomquist, J. D., & Sekellick, A. J. (2019). Toward Explaining Nitrogen and Phosphorus Trends in Chesapeake Bay Tributaries, 1992–2012. Journal of the American Water Resources Association, 55(5), 1149–1168. https://doi.org/10.1111/1752-1688.12756

Bailey, R. (2022). *GIS shape file of annual average groundwater head - CONUS*. https://doi.org/10.6084/m9.figshare.19441046

Bailey, R. T., Abbas, S., Arnold, J., White, M., Gao, J., & Čerkasova, N. (2023). Augmenting the National agroecosystem model with physically based spatially distributed groundwater modeling. *Environ. Model. SoftW*, *160*(November 2022). https://doi.org/10.1016/j.envsoft.2022.105589

Bailey, R. T., Bieger, K., Arnold, J. G., & Bosch, D. D. (2020). A new physically-based spatially-distributed groundwater flow module for SWAT+. *Hydrology*, *7*(4), 1–23. https://doi.org/10.3390/hydrology7040075

Bailey, R. T., Park, S., Bieger, K., Arnold, J. G., & Allen, P. M. (2020). Enhancing SWAT+ simulation of groundwater flow and groundwater-surface water interactions using MODFLOW routines. *Environ. Model. SoftW*, *126*(September 2019), 104660. https://doi.org/10.1016/j.envsoft.2020.104660

Baker, T. J., & Miller, S. N. (2013). Using the Soil and Water Assessment Tool (SWAT) to assess land use impact on water resources in an East African watershed. *J. Hydrol.*, *486*, 100–111. https://doi.org/10.1016/j.jhydrol.2013.01.041

Beck, M. W., & Murphy, R. R. (2017). Numerical and Qualitative Contrasts of Two Statistical Models for Water Quality Change in Tidal Waters. Journal of the American Water Resources Association, 53(1), 197–219. https://doi.org/10.1111/1752-1688.12489

Beegle, D. (2013). Nutrient Management and the Chesapeake Bay. *J. contemp. water res. educ.*, *151*(1), 3–8. https://doi.org/10.1111/j.1936-704x.2013.03146.x

Bhatt, G., Linker, L., Shenk, G., Bertani, I., Tian, R., Rigelman, J., Hinson, K., & Claggett, P. (2023). Water quality impacts of climate change, land use, and population growth in the Chesapeake Bay watershed. *J Am Water Resour Assoc*, *June*, 1–29. https://doi.org/10.1111/1752-1688.13144

Bieger, K., Arnold, J. G., Rathjens, H., White, M. J., Bosch, D. D., Allen, P. M., Volk, M., & Srinivasan, R. (2017). Introduction to SWAT+, A Completely Restructured Version of the Soil and Water Assessment Tool. *J Am Water Resour Assoc*, *53*(1), 115–130. https://doi.org/10.1111/1752-1688.12482

Brakebill, J. W., Ator, S. W., & Schwarz, G. E. (2010). Sources of suspended-sediment flux in streams of the chesapeake bay watershed: A regional application of the sparrow model. Journal of the American Water Resources Association, 46(4), 757–776. https://doi.org/10.1111/j.1752-1688.2010.00450.x

Buonocore, C., Gomiz Pascual, J. J., Pérez Cayeiro, M. L., Mañanes Salinas, R., & Bruno Mejías, M. (2021). Modelling the impacts of climate and land use changes on water quality in the Guadiana basin and the adjacent coastal area. *Sci. Total Environ.*, *776*, 146034. https://doi.org/10.1016/j.scitotenv.2021.146034

Camara, M., Jamil, N. R., & Abdullah, A. F. Bin. (2019). Impact of land uses on water quality in Malaysia: a review. *Ecol. Process.*, *8*(1). https://doi.org/10.1186/s13717-019-0164-x

Clune, J. W., Capel, P. D., Miller, M. P., Burns, D. A., Sekellick, A. J., Claggett, P. R., Coupe, R. H., Fanelli, R. M., Garcia, A. M., Raffensperger, J. P., Terziotti, S., Bhatt, G., Blomquist, J. D., Hopkins, K. G., Keisman, J. L., Linker, L. C., Shenk, G. W., Smith, R. A., Soroka, A. M., … Zhang, Q. (2021). Nitrogen in the Chesapeake Bay Watershed A Century of Change 1950-2050. *US Geological Survey Circular*, *1486*, 1–180. https://doi.org/10.3133/cir1486

Dieter, C. A., Maupin, M. A., Caldwell, R. R., Harris, M. A., Ivahnenko, T. I., Lovelace, J. K., Barber, N. L., & Linsey,

K. S. (2018). Estimated use of water in the United States in 2015. In *Circular*. https://doi.org/10.3133/cir1441

Doherty, J. E., Hunt, R. J., & Tonkin, M. J. (2010). *Approaches to Highly Parameterized Inversion : A Guide to Using PEST for Model-Parameter and Predictive-Uncertainty Analysis: U.S. Geological Survey Scientific Investigations Report 2010 – 5211*. 71.

Du, J., Shen, J., Park, K., Wang, Y. P., & Yu, X. (2018). Worsened physical condition due to climate change contributes to the increasing hypoxia in Chesapeake Bay. *Sci. Total Environ.*, *630*, 707–717. https://doi.org/10.1016/j.scitotenv.2018.02.265

Duda, P. B., Hummel, P. R., Jr., A. S. D., & Imhoff, J. C. (2012). BASINS/HSPF: Model Use, Calibration, and Validation. *Trans. ASABE*, *55*(4), 1523–1547. https://doi.org/10.13031/2013.42261

El-Khoury, A., Seidou, O., Lapen, D. R. L., Que, Z., Mohammadian, M., Sunohara, M., & Bahram, D. (2015). Combined impacts of future climate and land use changes on discharge, nitrogen and phosphorus loads for a Canadian river basin. *J. Environ. Manage.*, *151*, 76–86. https://doi.org/10.1016/j.jenvman.2014.12.012

Gémesi, Z., Downing, J. A., Cruse, R. M., & Anderson, P. F. (2011). Effects of watershed configuration and composition on downstream lake water quality. *J. Environ. Qual.*, *40*(2), 517–527. https://doi.org/10.2134/jeq2010.0133

Gesch, D. B., Evans, G. A., Oimoen, M. J., & Arundel, S. (2018). *The National Elevation Dataset* (pp. 83–110). American Society for Photogrammetry and Remote Sensing. https://pubs.usgs.gov/publication/70201572

Hawkins, T. W. (2015). Simulating the Impacts of Projected Climate Change on Streamflow Hydrology for the Chesapeake Bay Watershed. *Ann Assoc Am Geogr*, *105*(4), 627–648. https://doi.org/10.1080/00045608.2015.1039108

Horton, J. D. (2017). *The state geologic map compilation (SGMC) geodatabase of the conterminous United States*.

Jordan, T. E., Weller, D. E., & Pelc, C. E. (2018). Effects of Local Watershed Land Use on Water Quality in Mid-Atlantic Coastal Bays and Subestuaries of the Chesapeake Bay. *Estuaries and Coasts*, *41*(2018), 38–53. https://doi.org/10.1007/s12237-017-0303-5

Kalcic, M. M., Muenich, R. L., Basile, S., Steiner, A. L., Kirchhoff, C., & Scavia, D. (2019). Climate Change and Nutrient Loading in the Western Lake Erie Basin: Warming Can Counteract a Wetter Future. *Environ. Sci. Technol.*, *53*(13), 7543–7550. https://doi.org/10.1021/acs.est.9b01274

Khoi, D. N., Nyugen, V. T., Sam, T. T., & Nhi, P. T. T. (2019). *Evaluation on Effects of Climate and Land-Use*

Changes on Streamflow and Water Quality in the La Buong River Basin, Southern Vietnam _ Enhanced Reader.pdf.

Kiprotich, P., Wei, X., Zhang, Z., Ngigi, T., Qiu, F., & Wang, L. (2021). Assessing the impact of land use and climate change on surface runoff response using gridded observations and swat+. *Hydrology*, *8*(1), 1–29. https://doi.org/10.3390/hydrology8010048

Liu, Z. J., Weller, D. E., Correll, D. L., & Jordan, T. E. (2000). Effects of land cover and geology on stream chemistry in watersheds of Chesapeake Bay. *J. Am. Water Resour. Assoc.*, *36*(6), 1349–1365. https://doi.org/10.1111/j.1752-1688.2000.tb05731.x

Mehdi, B., Ludwig, R., & Lehner, B. (2015). Evaluating the impacts of climate change and crop land use change on streamflow , nitrates and phosphorus : A modeling study in Bavaria. *J. Hydrol. Reg. Stud.*, *4*, 60–90. https://doi.org/10.1016/j.ejrh.2015.04.009

Meier, H. E. M., Eilola, K., Almroth-Rosell, E., Schimanke, S., Kniebusch, M., Höglund, A., Pemberton, P., Liu, Y., Väli, G., & Saraiva, S. (2019). Disentangling the impact of nutrient load and climate changes on Baltic Sea hypoxia and eutrophication since 1850. *Climate Dynamics*, *53*(1–2), 1145–1166. https://doi.org/10.1007/s00382-018-4296-y

Miller, M. P., Capel, P. D., García, A. M., & Ator, S. W. (2020). Response of Nitrogen Loading to the Chesapeake Bay to Source Reduction and Land Use Change Scenarios: A SPARROW-Informed Analysis. Journal of the American Water Resources Association, 56(1), 100–112. https://doi.org/10.1111/1752-1688.12807

Modi, P. A., Fuka, D. R., & Easton, Z. M. (2021). Impacts of climate change on terrestrial hydrological components and crop water use in the Chesapeake Bay watershed. *J. Hydrol. Reg. Stud.*, *35*(May), 100830. https://doi.org/10.1016/j.ejrh.2021.100830

Moore, R. B., & Dewald, T. G. (2016). The Road to NHDPlus — Advancements in Digital Stream Networks and Associated Catchments. *J Am Water Resour Assoc*, *52*(4), 890–900. https://doi.org/10.1111/1752-1688.12389

Mukundan, R., Hoang, L., Gelda, R. K., Yeo, M. H., & Owens, E. M. (2020). Climate change impact on nutrient loading in a water supply watershed. *J. Hydrol*, *586*(March), 124868. https://doi.org/10.1016/j.jhydrol.2020.124868

Murphy, R. R., Perry, E., Harcum, J., & Keisman, J. (2019). A Generalized Additive Model approach to evaluating water quality: Chesapeake Bay case study. Environmental Modelling and Software, 118(April), 1–13.

https://doi.org/10.1016/j.envsoft.2019.03.027

Najjar, R. G., Pyke, C. R., Adams, M. B., Breitburg, D., Hershner, C., Kemp, M., Howarth, R., Mulholland, M. R., Paolisso, M., Secor, D., Sellner, K., Wardrop, D., & Wood, R. (2010). Potential climate-change impacts on the Chesapeake Bay. *Estuarine, Coast. Shelf Sci*, *86*(1), 1–20. https://doi.org/10.1016/j.ecss.2009.09.026

Nkwasa, A., Chawanda, C. J., Jägermeyr, J., & van Griensven, A. (2022). Improved representation of agricultural land use and crop management for large-scale hydrological impact simulation in Africa using SWAT+. *Hydrol Earth Syst Sci.*, *26*(1), 71–89. https://doi.org/10.5194/hess-26-71-2022

Oelsner, G. P., & Stets, E. G. (2019). Recent trends in nutrient and sediment loading to coastal areas of the conterminous U.S.: Insights and global context. *Sci. Total Environ.*, *654*, 1225–1240. https://doi.org/10.1016/j.scitotenv.2018.10.437

Paul, M., Dangol, S., Kholodovsky, V., Sapkota, A. R., Negahban-Azar, M., & Lansing, S. (2020). Modeling the impacts of climate change on crop yield and irrigation in the monocacy river watershed, usa. *Climate*, *8*(12), 1–20. https://doi.org/10.3390/cli8120139

Pihlainen, S., Zandersen, M., Hyytiäinen, K., Andersen, H. E., Bartosova, A., Gustafsson, B., Jabloun, M., McCrackin, M., Meier, H. E. M., Olesen, J. E., Saraiva, S., Swaney, D., & Thodsen, H. (2020). Impacts of changing society and climate on nutrient loading to the Baltic Sea. *Sci. Total Environ.*, *731*. https://doi.org/10.1016/j.scitotenv.2020.138935

Preston, S. D., Alexander, R. B., Woodside, M. D., & Hamilton, P. A. (2009). SPARROW modeling -- Enhancing understanding of the Nation's water quality. U.S. Geological Survey Fact Sheet, 2009–3019, 6. https://pubs.usgs.gov/fs/2009/3019/pdf/fs_2009_3019.pdf

Pulighe, G., Lupia, F., Chen, H., & Yin, H. (2021). Modeling climate change impacts on water balance of a mediterranean watershed using swat+. *Hydrology*, *8*(4), 1–14. https://doi.org/10.3390/hydrology8040157

Rabalais, N. N., Turner, R. E., Díaz, R. J., & Justić, D. (2009). Global change and eutrophication of coastal waters. *ICES J. Mar. Sci.*, *66*(7), 1528–1537. https://doi.org/10.1093/icesjms/fsp047

Sanford, W. E., Pope, J. P., Selnick, D. L., & Stumvoll, R. F. (2012). *Simulation of Groundwater Flow in the Shallow Aquifer System of the Delmarva Peninsula, Maryland and Delaware*. 68. https://pubs.usgs.gov/of/2012/1140/pdf/OFR_2012-1140.pdf

Sarkar, S., Yonce, H. N., Keeley, A., Canfield, T. J., Butcher, J. B., & Paul, M. J. (2019). Integration of SWAT and

HSPF for Simulation of Sediment Sources in Legacy Sediment-Impacted Agricultural Watersheds. Journal of the American Water Resources Association, 55(2), 497–510. https://doi.org/10.1111/1752-1688.12731

Seong, C., & Sridhar, V. (2017). Hydroclimatic variability and change in the Chesapeake Bay watershed. *J. Water Clim. Change*, *8*(2), 254–273. https://doi.org/10.2166/wcc.2016.008

Shangguan, W., Hengl, T., Mendes de Jesus, J., Yuan, H., & Dai, Y. (2017). Mapping the global depth to bedrock for land surface modeling. *J. Adv. Model. Earth Syst.*, *9*(1), 65–88. https://doi.org/10.1002/2016MS000686

Shenk, G. W., & Linker, L. C. (2013). Development and application of the 2010 Chesapeake Bay Watershed total maximum daily load model. Journal of the American Water Resources Association, 49(5), 1042–1056. https://doi.org/10.1111/jawr.12109

Shrestha, M. K., Recknagel, F., Frizenschaf, J., & Meyer, W. (2017a). Future climate and land uses effects on flow and nutrient loads of a Mediterranean catchment in South Australia. *Sci. Total Environ.*, *590–591*, 186–193. https://doi.org/10.1016/J.SCITOTENV.2017.02.197

Shrestha, M. K., Recknagel, F., Frizenschaf, J., & Meyer, W. (2017b). Future climate and land uses effects on flow and nutrient loads of a Mediterranean catchment in South Australia. *Sci. Total Environ.*, *590–591*, 186–193. https://doi.org/10.1016/j.scitotenv.2017.02.197

Shrestha, R. R., Dibike, Y. B., & Prowse, T. D. (2012). Modelling of climate-induced hydrologic changes in the Lake Winnipeg watershed. *J. Gt. Lakes Res*, *38*(SUPPL. 3), 83–94. https://doi.org/10.1016/J.JGLR.2011.02.004

Shrestha, S., Bhatta, B., Shrestha, M., & Shrestha, P. K. (2018). Integrated assessment of the climate and landuse change impact on hydrology and water quality in the Songkhram River Basin, Thailand. *Sci. Total Environ.*, *643*, 1610–1622. https://doi.org/10.1016/j.scitotenv.2018.06.306

Sinha, E., Michalak, A. M., & Balaji, V. (2017). Eutrophication will increase during the 21st century as a result of precipitation changes. *Science*, *357*(6349), 1–5. https://doi.org/10.1126/science.aan2409

Skinner, K. D., & Maupin, M. A. (2019). Point-source nutrient loads to streams of the conterminous United States, 2012. In *Data Series*. https://doi.org/10.3133/ds1101

Srinivasan, R., Arnold, J. G., & Jones, C. A. (1998). Hydrologic Modelling of the United States with the Soil and Water Assessment Tool. *Int. J. Water Resour. Dev.*, *14*, 3–15. https://doi.org/10.1080/07900629849231

Tu, J. (2009). Combined impact of climate and land use changes on streamflow and water quality in eastern Massachusetts, USA. *J. Hydrol*, *379*(3–4), 268–283. https://doi.org/10.1016/j.jhydrol.2009.10.009

Ullman, W. J., Voynova, Y. G., Andres, A. S., & Survey, D. G. (2013). *Report of Investigations Nanticoke at Bridgeville Project The Determination of Total Nutrient Loads from the Nanticoke Watershed above the USGS Nanticoke River near Bridgeville Gauging Site (USGS 01487000) from Data Provided by an Automated Nutrient Ana*. *December*.

Valayamkunnath, P., Barlage, M., Chen, F., Gochis, D. J., & Franz, K. J. (2020). Mapping of 30-meter resolution tile-drained croplands using a geospatial modeling approach. *Scientific Data*, *7*(1), 257.

Wagena, M. B., Collick, A. S., Ross, A. C., Najjar, R. G., Rau, B., Sommerlot, A. R., Fuka, D. R., Kleinman, P. J. A., & Easton, Z. M. (2018). Impact of climate change and climate anomalies on hydrologic and biogeochemical processes in an agricultural catchment of the Chesapeake Bay watershed, USA. *Sci. Total Environ.*, *637–638*, 1443–1454. https://doi.org/10.1016/j.scitotenv.2018.05.116

Wei, X., & Bailey, R. T. (2021). Evaluating nitrate and phosphorus remediation in intensively irrigated stream-aquifer systems using a coupled flow and reactive transport model. *J. Hydrol*, *598*, 126304. https://doi.org/10.1016/J.JHYDROL.2021.126304

Wei, X., Bailey, R. T., Records, R. M., Wible, T. C., & Arabi, M. (2019). Comprehensive simulation of nitrate transport in coupled surface-subsurface hydrologic systems using the linked SWAT-MODFLOW-RT3D model. *Environ. Model. SoftW*, *122*, 104242. https://doi.org/10.1016/J.ENVSOFT.2018.06.012

Weller, D. E., & Baker, M. E. (2014). Cropland riparian buffers throughout chesapeake bay watershed: Spatial patterns and effects on nitrate loads delivered to streams. *J Am Water Resour Assoc*, *50*(3), 696–712. https://doi.org/10.1111/jawr.12207

Weller, D. E., Baker, M. E., & Jordan, T. E. (2011). Effects of riparian buffers on nitrate concentrations in watershed discharges: New models and management implications. *Ecol. Appl.*, *21*(5), 1679–1695. https://doi.org/10.1890/10-0789.1

White, M. J., Arnold, J. G., Bieger, K., Allen, P. M., Gao, J., Čerkasova, N., Gambone, M., Park, S., Bosch, D. D., Yen, H., & Osorio, J. M. (2022). Development of a Field Scale SWAT+ Modeling Framework for the Contiguous U.S. *J Am Water Resour Assoc*, *58*(6), 1545–1560. https://doi.org/10.1111/1752-1688.13056

Wu, J., Yen, H., Arnold, J. G., Yang, Y. C. E., Cai, X., White, M. J., Santhi, C., Miao, C., & Srinivasan, R. (2020). Development of reservoir operation functions in SWAT+ for national environmental assessments. *J. Hydrol*, *583*(December 2019), 124556. https://doi.org/10.1016/j.jhydrol.2020.124556

Wurtsbaugh, W. A., Paerl, H. W., & Dodds, W. K. (2019). Nutrients, eutrophication and harmful algal blooms along the freshwater to marine continuum. *Wiley Interdisciplinary Reviews: Water*, *6*(5), 1–27. https://doi.org/10.1002/WAT2.1373

Yan, L., & Roy, D. P. (2016). Conterminous United States crop field size quantification from multi-temporal Landsat data. *Remote Sens. Environ.*, *172*, 67–86. https://doi.org/10.1016/j.rse.2015.10.034

Yimer, E. A., Bailey, R. T., Piepers, L. L., Nossent, J., & Griensven, A. Van. (2023). Improved Representation of Groundwater–Surface Water Interactions Using SWAT+gwflow and Modifications to the gwflow Module. *Water 2023, Vol. 15, Page 3249*, *15*(18), 3249. https://doi.org/10.3390/W15183249